RadioGraphics

Novel Oncologic Drugs: What They Do and How They Affect Images[1]

Roberto García Figueiras, MD • Anwar R. Padhani, MBBS, FRCP, FRCR Vicky J. Goh, MD, MRCP, FRCR • Joan C. Vilanova, MD, PhD • Sandra Baleato González, MD • Carmen Villalba Martín, MD • Antonio Gómez Caamaño, MD • Anaberta Bermúdez Naveira, MD • Peter L. Choyke, MD

CME FEATURE

See www.rsna.org/education/rg_cme.html

LEARNING OBJECTIVES FOR TEST 5

After completing this journal-based CME activity, participants will be able to:

- Describe the spectrum of targeted therapies used in cancer treatment and their different mechanisms of action.
- List the limitations of conventional imaging techniques and current response criteria for evaluation of targeted therapies.
- Discuss the role of functional and molecular imaging techniques in evaluation of tumor response to targeted therapies.

TEACHING POINTS

See last page

Targeted therapies are designed to interfere with specific aberrant biologic pathways involved in tumor development. The main classes of novel oncologic drugs include antiangiogenic drugs, antivascular agents, drugs interfering with EGFR-HER2 or KIT receptors, inhibitors of the PI3K/Akt/mTOR pathway, and hormonal therapies. Cancer cells usurp normal signal transduction pathways used by growth factors to stimulate proliferation and sustain viability. The interaction of growth factors with their receptors activates different intracellular pathways affecting key tumor biologic processes such as neoangiogenesis, tumor metabolism, and tumor proliferation. The response of tumors to anticancer therapy can be evaluated with anatomic response assessment, qualitative response assessment, and response assessment with functional and molecular imaging. Angiogenesis can be measured by means of perfusion imaging with computed tomography and magnetic resonance (MR) imaging. Diffusion-weighted MR imaging allows imaging evaluation of tumor cellularity. The main imaging techniques for studying tumor metabolism in vivo are positron emission tomography and MR spectroscopy. Familiarity with imaging findings secondary to tumor response to targeted therapies may help the radiologist better assist the clinician in accurate evaluation of tumor response to these anticancer treatments. Functional and molecular imaging techniques may provide valuable data and augment conventional assessment of tumor response to targeted therapies. Supplemental material available at *http://radiographics.rsna.org/lookup/suppl/doi:10.1148/rg.317115108/-/DC1*.

Abbreviations: ADC = apparent diffusion coefficient, DCE = dynamic contrast-enhanced, EGFR = epidermal growth factor receptor, FDG = fluorine 18 fluorodeoxyglucose, FLT = fluorine 18 fluorothymidine, GIST = gastrointestinal stromal tumor, HER2 = human epidermal growth factor receptor 2, HIF = hypoxia-inducible factor, MIP = maximum intensity projection, mTOR = mammalian target of rapamycin, NOD = novel oncologic drug, PDGF = platelet-derived growth factor, PI3K = phosphatidylinositol 3-kinase, RECIST = Response Evaluation Criteria in Solid Tumors, SUV = standardized uptake value, VDA = vascular disrupting agent, VEGF = vascular endothelial growth factor, VEGFR = VEGF receptor

RadioGraphics 2011; 31:2059–2091 • **Published online** 10.1148/rg.317115108 • **Content Codes:** BQ MI OI

[1]From the Departments of Radiology (R.G.F., S.B.G., C.V.M., A.B.N.) and Radiotherapy (A.G.C.), Grupo de Imagen Molecular, Fundación IDI-CHUS/IDIS, Complexo Hospitalario Universitario de Santiago de Compostela, Choupana s/n, 15702 Santiago de Compostela, Spain; Paul Strickland Scanner Centre, Mount Vernon Cancer Centre, Northwood, Middlesex, England (A.R.P.); Division of Imaging Sciences and Biomedical Engineering, King's College London, London, England (V.J.G.); Department of Radiology, Clínica Girona and Hospital Santa Caterina, Girona, Spain (J.C.V.); and Center for Cancer Research, National Cancer Institute, National Institutes of Health, Bethesda, Md (P.L.C.). Recipient of a Magna Cum Laude award for an education exhibit at the 2010 RSNA Annual Meeting. Received May 3, 2011; revision requested June 27 and received July 14; accepted July 25. For this journal-based CME activity, the authors A.R.P., V.J.G., and J.C.V. have disclosed various financial relationships (see p 2088); all other authors, the editor, and reviewers have no relevant relationships to disclose. **Address correspondence to** R.G.F. (e-mail: *roberto.garcia.figueiras@sergas.es*).

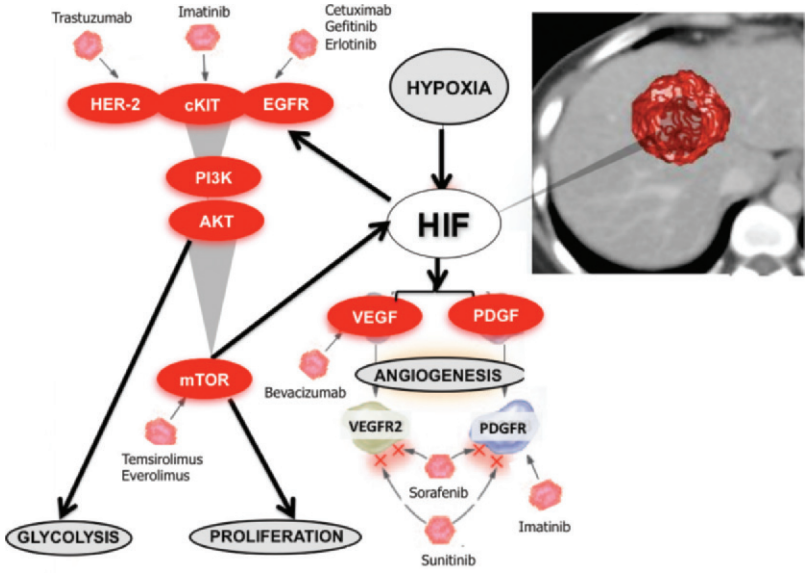

Figure 1. Relationship between transduction pathways and tumor hallmarks and specific biologic pathways targeted and disrupted by NODs. Akt is a serine-threonine protein kinase, cKIT is a proto-oncogene. *EGFR* = epidermal growth factor receptor, *HER2* = human epidermal growth factor receptor 2, *HIF* = hypoxia-inducible factor, *mTOR* = mammalian target of rapamycin, *PDGF* = platelet-derived growth factor, *PDGFR* = PDGF receptor, *PI3K* = phosphatidylinositol 3-kinase, *VEGF* = vascular endothelial growth factor, *VEGFR* = VEGF receptor.

Introduction

Recent advances in molecular biology have dramatically accelerated our understanding of how cancer develops, grows, and spreads, thus creating great expectations for translating new discoveries into effective treatments for patients. Over the past decade, there has been an increase in knowledge about pathophysiologic processes that are common to most tumors. Typical hallmarks of tumors include *(a)* independence from growth signals, *(b)* insensitivity to growth-inhibitory signals, *(c)* evasion of apoptosis, *(d)* development of a limitless potential for replication, *(e)* development of sustained angiogenesis, and *(f)* tissue invasion and metastasis. These hallmarks of cancer are caused by dysregulation of cell control pathways, which in cancers also results in an abnormal microenvironment (1).

Teaching Point

As a consequence, there has been an emergence of a wide range of novel oncologic drugs (NODs) designed to target and disrupt specific biologic pathways (Fig 1). In general, these agents use different strategies to block specific biologic targets (2,3) (Fig 2). In current clinical practice, the main classes of NODs include antiangiogenic drugs, antivascular agents, drugs interfering with EGFR-HER2 or KIT receptors, PI3K/Akt/mTOR pathway inhibitors, and hormonal therapies, although the latter constitute a specific class of therapies (4) (Table 1).

Teaching Point

In this article, we review the spectrum of NODs (which show mainly a cytostatic effect) and their different mechanisms of action. In addition, the limitations of conventional imaging techniques and current response criteria for evaluating these drugs are described. The role of functional and molecular imaging techniques as a noninvasive and quantitative means to improve the evaluation of cancer patients treated with these therapies is discussed. Finally, we examine the evolving roles of these techniques and challenges for their implementation. Specific topics addressed are biologic pathways in cancer; response evaluation and oncologic drugs; imaging evaluation of angiogenesis, tumor cellularity, tumor metabolism, tumor proliferation, and hypoxia; assessment of NODs with imaging; and future challenges and opportunities.

Biologic Pathways in Cancer

Cancer cells usurp normal signal transduction pathways used by growth factors to stimulate proliferation and sustain viability. The interaction of growth factors with their receptors activates different intracellular pathways affecting key tumor biologic processes such as neoangiogenesis, tumor metabolism, and tumor proliferation. This relationship between transduction pathways and tumor hallmarks is an important element in understanding imaging findings in evaluation of the response to NODs (Table 2).

Angiogenesis

Neoangiogenesis, the formation of new blood vessels, is a multistep process regulated by pro- and antiangiogenic factors (5,6). This process is essential for solid tumor growth beyond 2–3 mm^3, when diffusion is no longer sufficient to

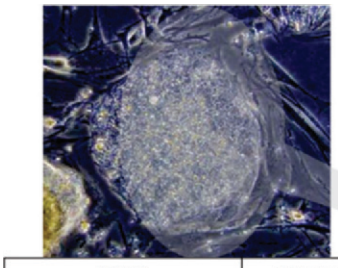

DRUG	MOLECULAR TARGET
MONOCLONAL ANTIBODIES blocking Growth Factors or Receptors	
Bevacizumab	VEGF
Cetuximab	EGFR (receptor HER-1)
Trastuzumab	receptor HER-2
TYROSINE KINASE inhibitors (TKIs)	
Sorafenib	VEGFR, PDGFR, C-KIT
Sunitinib	VEGFR, PDGFR, C-KIT
Erlotinib	EGFR
Gefitinib	EGFR
Imatinib	c-Kit

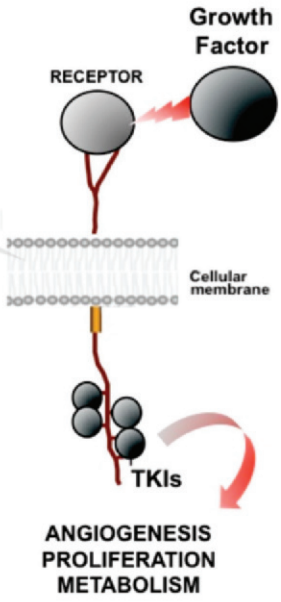

Figure 2. Strategies used to block specific biologic targets may act at different levels: growth factors, receptors, or tyrosine kinases. *HER-1* = human epidermal growth factor receptor 1.

Table 1
Functions of Biologic Pathways Targeted by NODs

Pathway	Action
VEGFR, PDGFR*	Activates malignant angiogenesis
EGFR-HER2	Activates proliferation, angiogenesis, invasion, metastasis, and evasion of apoptosis
PI3K/Akt/mTOR	Activates cancer cell growth and proliferation, evasion of apoptosis, synthesis of proteins necessary for cell growth, cell cycle progression, and cell metabolism
cKIT	Plays a critical role in cell proliferation and differentiation
Hormonal	Cell growth and survival

*PDGFR = PDGF receptor.

Table 2
Comparison of Cytotoxic Therapy versus NODs

Characteristics of Therapy	Chemotherapy	NODs
Tumoral effect	Cytotoxic	Mainly cytostatic
Criteria for patient selection	Histologic features of the tumor	Presence of the target in the tumor or molecular pathology
Criteria for tumor response	Tumor shrinkage	Tumor stabilization or shrinkage
Imaging techniques for response evaluation	Anatomic imaging to evaluate size and qualitative criteria (ie, tumor appearance)	Mainly, functional or molecular imaging techniques; anatomic imaging to evaluate size and qualitative criteria (ie, tumor appearance)
Time of response evaluation	Late (2 mo)	Early (2–6 wk)
Primary end points in drug development	Characterization of toxic effects and determination of dose-limiting toxic effects and maximum tolerated dose	Determination of target inhibition, biologically active, and optimal doses
Toxic effects of drugs	Usually nonspecific: multisystemic involvement	Less toxic: target-specific toxic effects

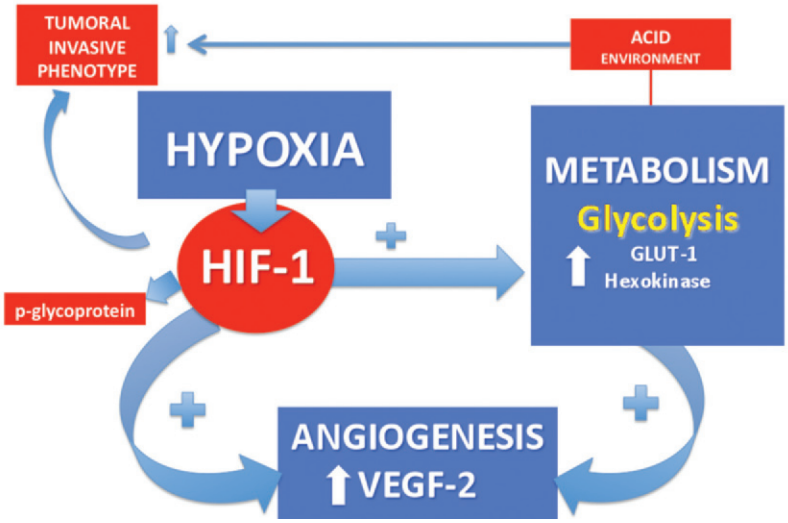

Figure 3. HIF-1 is a key feature in the hypoxia-mediated aggressive behavior of cancer cells and their resistance to therapy. HIF-1 stimulates a number of molecular events required for adaptation of tumor cells to hypoxia, including unregulated glycolysis (overexpression of membrane glucose transporters *[GLUT-1]* and increased hexokinase-2 activity), angiogenesis (increased VEGF), and mutant p-glycoprotein (resistance to radiation therapy and chemotherapy).

supply tumor cells with oxygen and nutrients. The primary stimulus for new vessel formation is presumed to be hypoxia induced by expansion of the growing cellular tumor mass. Hypoxia induces the expression of HIF, which promotes the expression of other factors, such as VEGF, PDGF, and carbonic anhydrase IX. In addition, hypoxia leads to resistance to radiation therapy and chemotherapy (p-glycoprotein), promotes tumor metabolism (glucose transporter GLUT-1) (7,8) (Fig 3), and enhances tumor progression.

Tumor angiogenesis provides an attractive target for anticancer therapy. There are two distinct approaches for antiangiogenesis therapy in tumors: angiogenesis inhibitors that inhibit the formation of new blood vessels by blocking the function of specific growth factors or receptors (eg, targeting VEGF-A) and vascular disrupting agents (VDAs) that target the established tumor vasculature, causing an acute shutdown of blood vessel flow and secondary tumor necrosis (6,9).

VEGF and its receptors are key regulators of normal angiogenesis and tumor angiogenesis. The major mediator of tumor angiogenesis is VEGF-A, also called VEGF, which signals through VEGFR-2, the major VEGF signaling receptor that mediates tumor angiogenesis. There is an upregulation of VEGF family members and the VEGF receptors in many different tumors (5,6,10), providing a viable target for antiangiogenesis therapy. Other angiogenic pathways, such as the placental growth factor receptor or the PDGF receptor, are also important for angiogenesis (11). PDGF is important for the recruitment of pericytes, which are required to stabilize microvessels (5,6,10,11). Different small-molecule tyrosine kinase receptor inhibitors may inhibit the action of both VEGF and PDGF.

VDAs target endothelial cells and pericytes of the tumor vasculature (9). Selective tumor vascular shutdown suggests that there are structural differences between tumor vessels and normal vessels. Many VDAs induce changes in the shape of endothelial cells by disruption of their cytoskeleton and cell-to-cell junctions. VDAs seem to be cytotoxic rather than cytostatic drugs, since their action results in an acute and pronounced shutdown of blood vessels, causing almost complete stoppage of blood flow and ultimately leading to central tumor necrosis.

Tumor Metabolism and Proliferation

Different pathways are involved in tumor proliferation and metabolic activity regulation. The majority of human epithelial cancers are marked by functional activation of growth factors and receptors of the EGFR family, including EGFR and HER2 (12–14). The two major intracellular pathways activated by EGFR-HER2 are the RAS-RAF-MEK-MAPK and the PI3K/Akt/mTOR pathways, which may result in cancer-cell proliferation, blocking of apoptosis, activation of invasion and metastasis, and stimulation of angiogenesis, cell metabolism, and synthesis of proteins necessary for cell growth. Moreover, different drugs such as everolimus or temsirolimus can specifically target the downstream signaling pathway PI3K/Akt/mTOR (15,16).

The KIT receptor also plays critical oncogenic roles in a broad spectrum of hematologic and solid tumors, controlling various cell processes like cell proliferation and differentiation, apoptosis, and metabolic tumor activity (17). Imatinib mesylate inhibits KIT kinase activity and represents the front-line drug for treatment of unresectable and advanced gastrointestinal stromal tumors (GISTs).

Table 3
Criteria for Tumor Response Evaluation

Criteria	Measurability of Target Lesions	Measurability of Nontarget Lesions	Response Evaluation
WHO (anatomic)*	Measurable bidimensionally (product of LD and greatest perpendicular diameter)	Nonmeasurable and nonevaluable (eg, lymphangitic pulmonary metastases, abdominal masses)	Change in sum of products of the LD and greatest perpendicular diameters of target lesions; no maximal number of lesions specified; CR = disappearance of all known disease, confirmed at 4 wk; PR = 50% decrease from baseline, confirmed at 4 wk; PD = 25% increase in one or more lesions or appearance of new lesions; NC = neither PR nor PD criteria met
RECIST 1.1 (anatomic)*	Measurable unidimensionally (LD only); size with conventional techniques = 20 mm, size with spiral CT = 10 mm, size of target lymph nodes = short axis ≥ 15 mm, size of nontarget lymph nodes = 10–15 mm, size of normal lymph nodes <10 mm	Nonmeasurable: all other lesions, including small lesions	Change in sum of LDs of target lesions (maximum of two per organ up to five total); CR = disappearance of all target lesions, confirmed at 4 wk; PR = 30% decrease from baseline, confirmed at 4 wk; PD = 20% increase over smallest sum observed and overall 5-mm net increase or appearance of new lesions; SD = neither PR nor PD criteria met
Choi (anatomic, qualitative)*	Attenuation (Hounsfield units) or unidimensional size	...	Change in size or attenuation of target lesions; CR = disappearance of all target lesions, confirmed at 4 wk; PR = 10% decrease in tumor size or 15% decrease in tumor attenuation at contrast material–enhanced CT, no new lesions, no obvious progression of nonmeasurable disease; PD = 10% increase in tumor size, tumor attenuation criteria for PR not met, new lesions; SD = neither PR nor PD criteria met

Note.—CMR = complete metabolic response, CR = complete response, CT = computed tomography, EORTC = European Organization for Research and Treatment of Cancer, FDG = fluorine 18 fluorodeoxyglucose, LD = longest dimension, NC = no change, PD = progressive disease, PERCIST = PET Response Criteria in Solid Tumors, PMD = progressive metabolic disease, PMR = partial metabolic response, PR = partial response, ROI = region of interest, SD = stable disease, SMD = stable metabolic disease, SUV = standardized uptake value, TLG = total lesion glycolysis, WHO = World Health Organization.
*The evaluation type is given in parentheses.

(continues)

Steroid hormone growth factors act in a different way, interacting with nuclear receptors directly to activate the transcription of genes whose products stimulate the growth and viability of hormone-dependent malignancies such as breast cancer and prostate cancer (3,18,19). Therapy of breast cancer is dominated by use of estrogen receptor antagonists, such as tamoxifen, or by depletion of estrogens with aromatase inhibitors, while hormonal therapy in prostate cancer is based on androgen blockade.

A detailed review of these pathways is beyond the scope of this article. However, it seems clear that they show several interactions that may explain the emergence of therapy resistance in cancer, making evaluation of drug effects a complex process, since different growth factors may converge across the same final pathway and one single drug may interact with diverse pathways.

Response Evaluation and Oncologic Drugs

Anatomic Response Assessment

When evaluating the response of tumors to anticancer therapy, a reliable and standardized methodology is essential, not only in daily patient care but also in clinical research. Anatomic objective response evaluation criteria based on assessment of the size of the tumor or metastases, such as the World Health Organization criteria or the Response Evaluation Criteria in Solid Tumors (RECIST), have been developed (20) (Table 3).

RECIST uses unidimensional measurements of the sum of the longest lesion diameters. The RECIST guidelines show some limitations for

Table 3
Criteria for Tumor Response Evaluation (*continued*)

Criteria	Measurability of Target Lesions	Measurability of Nontarget Lesions	Response Evaluation
EORTC (molecular)*	Tumor regions defined on pretreatment scans should be drawn on region of high fluorine 18 FDG uptake representing viable tumor; whole tumor uptake should also be recorded	...	Change in SUV of target lesions; CMR = complete resolution of FDG uptake in tumor volume so that it is indistinguishable from surrounding normal tissue; PMR = minimum of 15% ± 25 decrease in tumor FDG SUV after one cycle of chemotherapy or >25% decrease after more than one treatment cycle (reduction in extent of tumor FDG uptake is not a requirement); PMD = >25% increase in tumor FDG SUV in tumor region defined on baseline scan, visible increase in extent of tumor FDG uptake (20% in LD), or appearance of new FDG uptake in metastatic lesions; SMD = <25% increase or <15% decrease in tumor FDG SUV and no visible increase in extent of tumor FDG uptake (20% in LD)
PERCIST (molecular)*	Measurable target lesion is hottest single tumor lesion SUV of "maximal 1.2-cm diameter volume ROI in tumor" (SUV peak); SUV peak is at least 1.5-fold greater than mean liver SUV + 2 standard deviations in normal right lobe if liver is normal	...	Change in SUV of target lesions; CMR = complete resolution of FDG uptake in measurable target lesion so that it is less than mean liver activity and indistinguishable from surrounding background blood pool levels, disappearance of all other lesions to background blood pool levels, no new FDG-avid lesions in pattern typical of cancer (if progression according to RECIST, must verify with follow-up); PMR = minimum 30% decrease in measurable target tumor FDG SUV peak with absolute decrease in SUV of at least 0.8 SUV units,† no increase >30% in SUV or size of target or nontarget lesions; PMD = >30% increase in FDG SUV peak with >0.8 SUV unit increase in tumor SUV peak from the baseline scan in a pattern typical of tumor and not of infection or treatment effect, visible increase in the extent of FDG tumor uptake (75% in TLG volume) with no decline in SUV, or new FDG-avid lesions that are typical of cancer and not related to treatment effect or infection;‡ SMD = neither PMR nor PMD criteria met

Note.—CMR = complete metabolic response, CR = complete response, CT = computed tomography, EORTC = European Organization for Research and Treatment of Cancer, FDG = fluorine 18 fluorodeoxyglucose, LD = longest dimension, NC = no change, PD = progressive disease, PERCIST = PET Response Criteria in Solid Tumors, PMD = progressive metabolic disease, PMR = partial metabolic response, PR = partial response, ROI = region of interest, SD = stable disease, SMD = stable metabolic disease, SUV = standardized uptake value, TLG = total lesion glycolysis, WHO = World Health Organization.
*The evaluation type is given in parentheses.
†Measurement is commonly made in the same lesion that was measured at baseline but can be made in another lesion if that lesion was previously present and is the most active lesion after treatment.
‡PMD other than new visceral lesions should be confirmed at follow-up study within 1 mo unless PMD is also clearly associated with progressive disease according to RECIST 1.1.

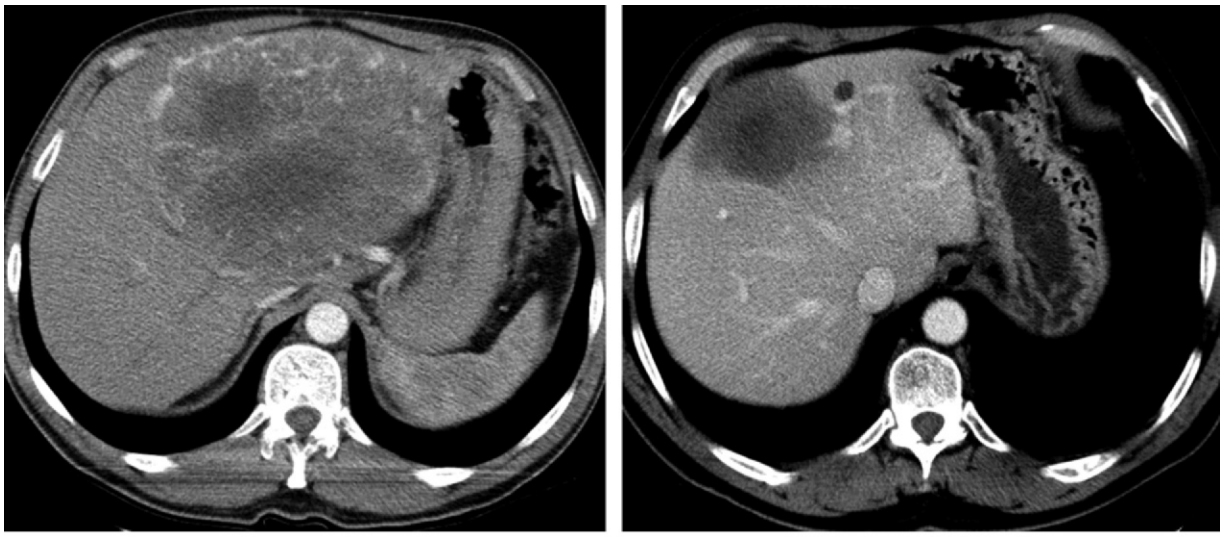

a. b.

Figure 4. GIST with liver metastases in a 52-year-old man. Axial contrast-enhanced CT images obtained before **(a)** and 3 months after **(b)** therapy with imatinib mesylate show a good response, with decreases in tumor size (>10%) and tumor attenuation (>15%).

evaluation of the treatment response of solid tumors, including tumors that cannot be measured, poor measurement reproducibility, and masses that persist after therapy (20–24). RECIST establishes fixed and forced categories that use size as the only criterion. These categories have been found to be not optimal for assessment of response in different malignancies, such as mesothelioma, prostate cancer, or pediatric malignancies (24).

Teaching Point

In addition, anatomic imaging techniques that use size-based criteria may be insensitive to changes that inform about the overall therapeutic success of cytostatic therapies, since the basic assumption that changes in tumor size reflect biologic activity is violated. Many targeted agents are cytostatic and therefore tumor shrinkage may not be seen. For example, it has been established that RECIST was less sensitive than the Choi criteria when monitoring GISTs treated with imatinib (23–25).

Moreover, numerous clinical studies show survival advantages for antiangiogenesis therapy with only modest anatomic responses for different tumors. In addition, the disconnection between anatomically determined progression-free survival and therapeutic efficacy (overall survival) is recognized for a number of cytostatic therapies (26). All of these features may establish the necessity for using different criteria and functional and molecular imaging techniques to evaluate tumor response to these therapies (4,24,26–31).

Qualitative Criteria for Response Assessment

The Choi criteria (Table 3) opened a new paradigm for tumor response and improved the accuracy of therapeutic response assessment (Fig 4). More recently, the value of changes in tumor attenuation and morphology, not accounted for in RECIST, has been demonstrated at contrast-enhanced CT in patients with metastatic colorectal cancer receiving bevacizumab and patients with renal carcinoma receiving tyrosine kinase receptor inhibitor therapy (32,33).

Among patients with liver metastases from colorectal cancer treated with bevacizumab-containing chemotherapy, CT-based morphologic criteria showed a statistically significant association with pathologic response and overall survival (Fig 5) (32). The Morphology, Attenuation, Size, and Structure criteria seem to be more accurate than RECIST, the modified Choi criteria, or size and attenuation CT criteria in assessment of the response of metastatic renal carcinoma to antiangiogenic targeted therapy with tyrosine kinase receptor inhibitors (33).

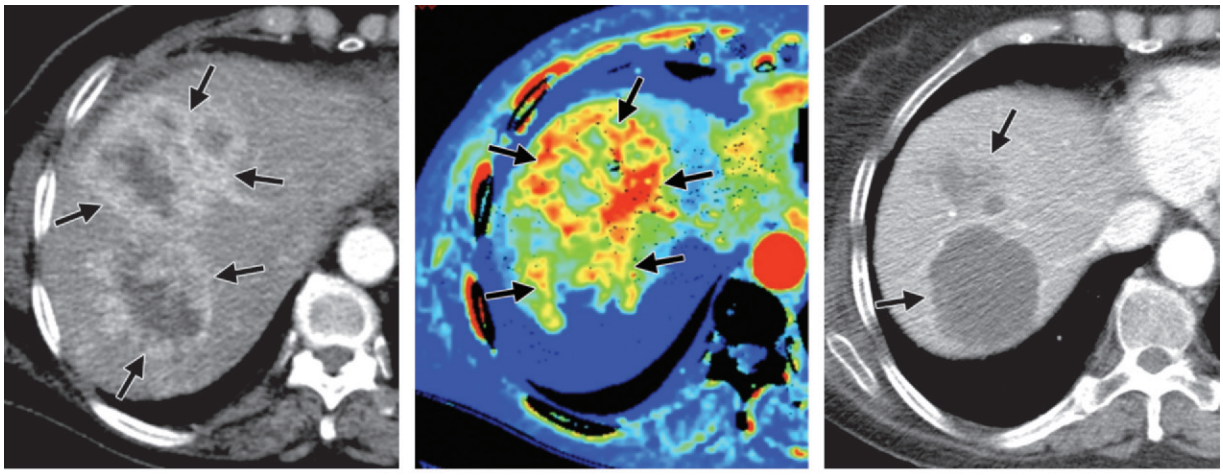

a. b. c.

Figure 5. Liver metastases from rectal cancer in a 63-year-old man. Axial CT image **(a)** and perfusion CT parametric map representing blood volume **(b)** obtained before therapy with bevacizumab and CT image obtained 2 weeks after therapy **(c)** show a morphologic incomplete response. After therapy, there is decreased attenuation in the peripheral rim-enhancing area compared with the pretherapy appearance (arrows in **a** and **b**). However, a discrete persistent ill-defined tumor-liver interface remains after treatment (arrows in **c**).

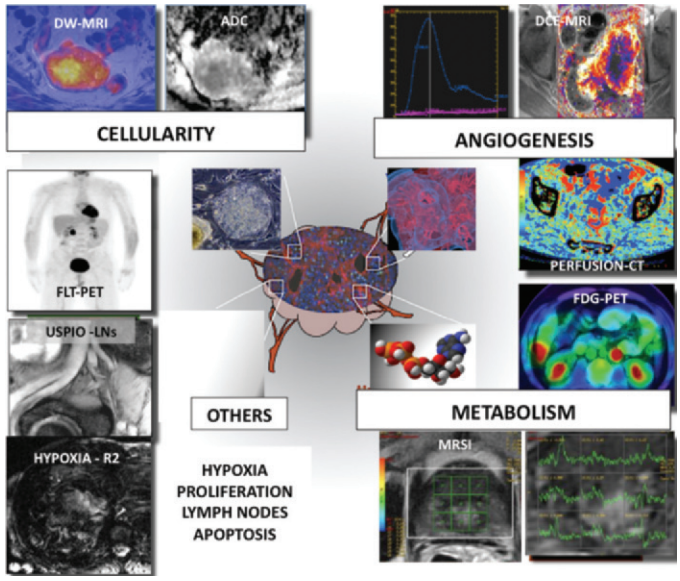

Figure 6. Functional and molecular imaging techniques for evaluation of tumor hallmarks. *ADC* = apparent diffusion coefficient, *DW* = diffusion-weighted, *FLT* = fluorine 18 fluorothymidine, *LNs* = lymph nodes, *MRSI* = MR spectroscopic imaging, *USPIO* = ultrasmall superparamagnetic iron oxide.

Response Assessment with Functional and Molecular Imaging

There has been a revolutionary improvement in imaging techniques. Medical imaging has evolved from a discipline focused on anatomy to one that can measure tissue function as well as specific molecular features (34–36). This has occurred mainly through advances in magnetic resonance (MR) imaging, positron emission tomography (PET), and CT. Functional and molecular imaging allows quantitative measurement of physiologic and molecular features of tumors by using noninvasive techniques (27).

Teaching Point

Functional imaging techniques, such as perfusion CT, dynamic susceptibility contrast MR imaging, dynamic contrast-enhanced (DCE) MR imaging, or diffusion-weighted MR imaging, provide information on tissue phenotype or behavior. Molecular imaging techniques, such as PET or MR spectroscopy, allow evaluation of cellular and molecular processes by measuring the levels or activities of specific macromolecules or metabolic pathways in vivo (Fig 6). Although these imaging techniques are based on different biologic properties, they can provide important quantitative imaging parameters that allow pathophysiologic correlation (Table 4).

Table 4
Overview of Functional and Molecular Imaging Techniques

Imaging Technique	Biologic Property on Which Imaging Is Based	Commonly Derived Quantitative Imaging Parameters or Biomarkers	Pathophysiologic Correlates
Diffusion-weighted MR imaging	Diffusivity of water, Brownian movement of water molecules	ADC, fractional anisotropy, water diffusivity, and perfusion fraction	Tissue architecture, including cell density, extracellular space tortuosity, gland formation, cell membrane integrity, fluid viscosity, and necrosis
DCE MR imaging	Contrast medium uptake rate in tissues, which is influenced by transfer rates, extracellular volume, and plasma volume fraction	Initial area under the gadolinium curve, transfer constant, rate constant, leakage space fraction, and fractional plasma volume	Vessel density, vascular permeability, perfusion, tissue cell fraction, and plasma volume
Dynamic susceptibility contrast-enhanced MR imaging	Blood flow, blood volume	Relative blood volume, relative blood flow, mean transit time, and vessel size index	Vessel density, vessel size, blood flow, and tumor grade
Dynamic CT (perfusion CT)	Contrast medium uptake rate in tissues, which is influenced by perfusion, vascular leakage, and vessel density	Blood flow, blood volume, mean transit time, permeability–surface area product, and extraction fraction	Vessel density, vascular permeability, perfusion pressure, and tumor grade
Hydrogen 1 MR spectroscopy	Cell membrane turnover and energetics, replacement of normal tissues	Quantified ratios of metabolites including choline and lipids	Tumor grade, proliferation index
Blood oxygen level–dependent or intrinsic susceptibility–weighted MR imaging	Deoxyhemoglobin shows higher relaxivity than oxyhemoglobin; measurements also reflect blood volume, perfusion, and the intrinsic composition of tissues	Intrinsic tissue relaxation rate (R2* = 1/T2*)	Ferromagnetic properties of tissues, level of tissue oxygenation
PET	Depends on the radiotracer	Mainly SUV; tissue-to-background ratio	...
FDG	Glucose metabolism	Mainly SUV; tissue-to-background ratio	Upregulation of GLUT-1 transporters and hexokinase II activity
FLT	Cellular proliferation	Mainly SUV; tissue-to-background ratio	Activity of cytosolic thymidine kinase 1, incorporation into newly synthesized DNA
Iodine 124 annexin-V	Apoptosis	Mainly SUV; tissue-to-background ratio	Exposure of phosphatidylserine in the cell membrane
^{18}F fluoromisonidazole and copper-diacetyl-bis(N4-methylthiosemicarbazone)	Tissue and cell oxygen tension	Mainly SUV; tissue-to-background ratio	Tissue oxygenation

Table 5
Dynamic Contrast-enhanced Imaging Techniques

Characteristics	2D or 3D T1-weighted DCE MR Imaging	2D T2*-weighted DCE MR Imaging	2D Single-Level Perfusion CT	3D Volume Perfusion CT	DCE US
Anatomic area	Body imaging, extravascular-extracellular space	Brain imaging, vascular space	Body imaging, extravascular-extracellular space	Body imaging, extravascular-extracellular space	Body imaging (mainly abdominal imaging), vascular space
Contrast material	Gadolinium (0.5 mmol/mL)	Gadolinium (0.5 mmol/mL)	Iodine (>300 mg/mL)	Iodine (>300 mg/mL)	Microbubbles (4–8 mL)
Dose	0.1 mmol/kg	0.2 mmol/kg	0.5 mL/kg	1 mL/kg	...
Injection rate	3 mL/sec bolus	4–6 mL/sec bolus	5–7 mL/sec bolus	2 mL/sec infusion	Bolus infusion
Volume (mL)	10–15	25–35	40–50	100	4–8
Acquisition type	Single-level	Single-level	Single-level	Multiple helical	Single-level
Z-axis coverage	3 × 8 mm, 12 × 3 mm	3 × 8 mm	Variable (number of detector rows, extended coverage techniques); 2–34 cm	Whole tumor	Whole tumor
Data sampling	Every 5–12 sec for 5–7 min	Every 1–2 sec for 1–2 min	Every 1 sec for 1–2 min	Every 1 sec for 1–2 min	4–6 min
Signal-to-noise ratio	Very high	Low	Low	Low	High
Analysis technique	General multicompartmental model	Central-volume theorem	Unicompartmental analysis, deconvolution, distributed parameter model	Patlak analysis	Dynamic flow harmonic method for detection of static or circulating microbubbles
Parameters	Qualitative: time–signal intensity curve; semiquantitative: initial area under the gadolinium curve; quantitative: transfer constant, leakage space, and rate constant	Relative blood flow, relative blood volume, and mean transit time	Qualitative: time-attenuation curve; quantitative: blood flow, blood volume, mean transit time, and permeability–surface area product	Qualitative: time-attenuation curve; quantitative: permeability–surface area product, blood volume	Qualitative: time-intensity curve; semiquantitative: peak intensity, time to peak intensity, mean transit time, coefficient of washout slope, area under the total curve, area under the curve during wash-in, and area under the curve during washout

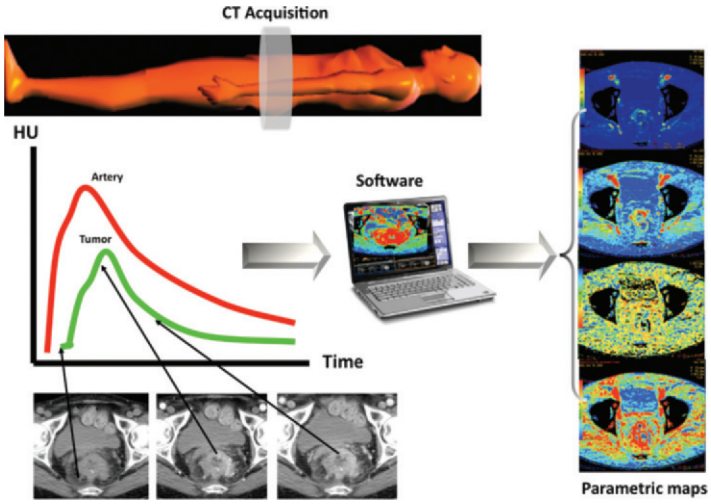

Figure 7. Overview of perfusion CT. During the image acquisition, the CT scanner measures the attenuation in a unit of volume versus time (ie, time-attenuation curve). The attenuation is directly proportional to the quantity of contrast agent present within the unit of volume. Software analysis uses a kinetic model to calculate the distribution of the contrast agent in the intravascular compartment and in the interstitial space, defining the parametric maps that characterize the perfusion in the tumor. *HU* = Hounsfield unit.

As a result, there has been increased use of functional and molecular imaging to demonstrate cancer hallmarks, such as angiogenesis and vascular function, metabolism, or cell density, that influence the progression and aggressiveness of the disease. Measurements of these parameters can be used in diagnosis and staging of cases of cancer, as well as for predicting and monitoring the therapeutic response of patients to both cytotoxic and cytostatic oncologic drugs.

Imaging Evaluation of Angiogenesis

Indirect measurement of angiogenesis can be performed noninvasively by using MR imaging, CT, ultrasonography (US), and PET (37–44), but perfusion imaging with CT and MR imaging is more useful in clinical practice. There are many different features of tumor vascularity (spatial heterogeneity and chaotic structure, high permeability to macromolecules, or heterogeneity of vascular density) that are characteristic of malignancy (45). These structural abnormalities of new tumor vessels lead to pathophysiologic changes within the tumor, including an increase in capillary permeability, volume of extravascular-extracellular space, and tumor perfusion, that permit distinction of malignant vascularity from benign vascularity with functional imaging techniques.

There are a few key differences when imaging tumor vascularity with the main functional imaging techniques used for studying angiogenesis: CT and MR imaging (46) (Table 5). Both techniques sequentially demonstrate passage of a bolus of contrast medium through a region of interest and allow quantification of the profile of tissue enhancement (Fig 7) (Movie E1 [online]). Dynamic CT techniques yield information based predominantly on the first pass of contrast material (absolute perfusion, blood volume). The most commonly used MR imaging technique (T1-weighted DCE imaging) may sample a volume of interest over a longer time and yields parameters that reflect microvessel perfusion, permeability, and extracellular leakage space.

In addition, dynamic MR imaging acquisitions allow calculation of semiquantitative parameters such as the initial area under the gadolinium curve or, by applying pharmacokinetic modeling, calculation of quantitative parameters such as the transfer constant (K^{trans}) and extravascular leakage space (v_e). CT techniques generate quantitative parameters such as relative blood volume, relative blood flow, and mean transit time. Although functional CT and MR imaging techniques have different physiologic bases, both types of parameters have been correlated with biologic surrogate markers of angiogenesis such as VEGF levels, tumor perfusion, and microvessel density (37–46).

Imaging Evaluation of Tumor Cellularity

Diffusion-weighted MR imaging is an emerging technique that allows detection and characterization of tissues because it incorporates sensitivity to water content and water movements into the images that are produced. Diffusion-weighted imaging reflects the effective thermal displacement of water molecules allowed to migrate for a given time. In biologic tissues, the movement of water molecules is restricted because their motion is influenced and limited by interactions with cell membranes and macromolecules (47–49). Diffusion-weighted imaging does not expose patients to ionizing radiation and no injection of isotopes or any other contrast medium is necessary. Diffusion-weighted imaging allows better detection and characterization of tumors than do morphologic sequences. The basic biologic premise is that malignant tissues are generally more cellular than

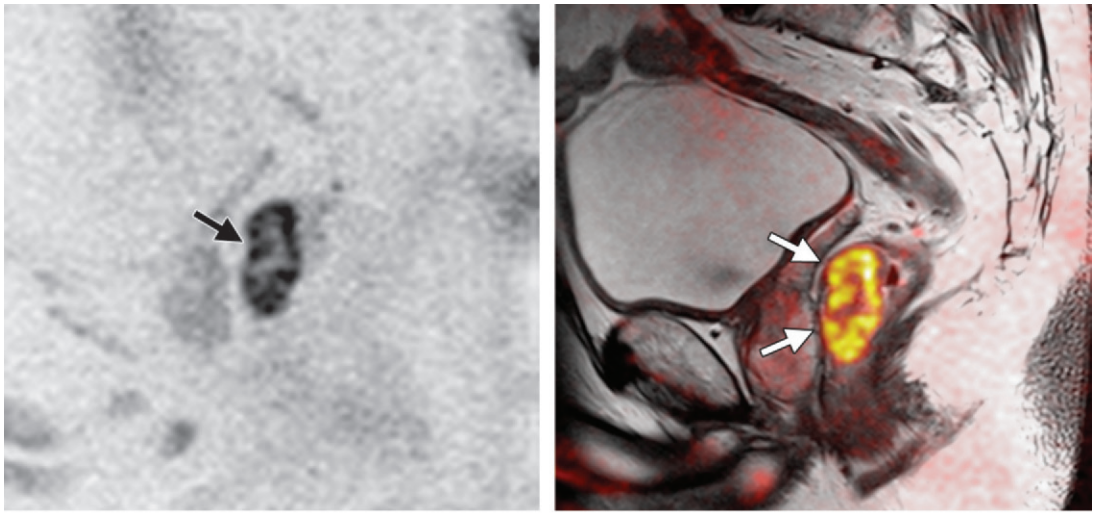

a. b.

Figure 8. Rectal cancer in a 58-year-old man. **(a)** Sagittal diffusion-weighted image obtained with a high *b* value (800 sec/mm^2) and an inverted gray scale shows a rectal tumor (arrow). **(b)** Fused image superimposing a sagittal T2-weighted MR image and a color-coded map derived from a high *b* value diffusion-weighted image clearly shows the rectal carcinoma (arrows).

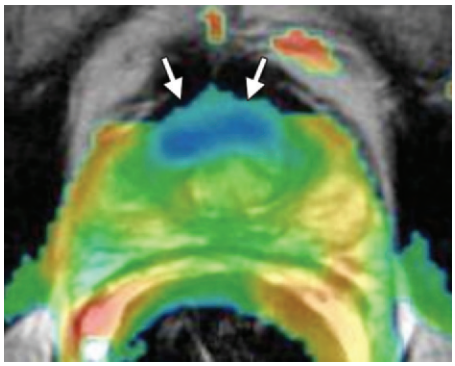

Figure 9. Prostate cancer in a 72-year-old man. Color-coded ADC parametric map (blue = low ADC values) shows a tumor (arrows) with low ADC values in the anterior part of the prostate gland.

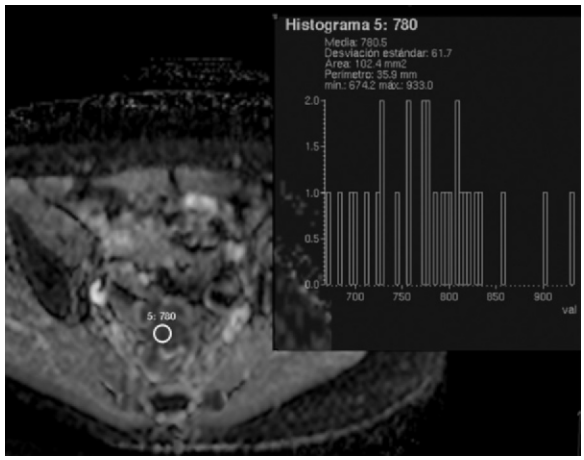

Figure 10. Rectal cancer. Axial diffusion-weighted image and ADC parametric map show a region of interest with a mean ADC value of 0.78 × 10^{-3} mm^2/sec. The ADC map histogram is a better representation of intratumor heterogeneity within pixels that have an ADC value of 1.0 × 10^{-3} mm^2/sec, while others have an ADC value of 0.6 × 10^{-3} mm^2/sec. *max* = maximum, *min* = minimum.

benign or normal tissues; therefore, water diffusion is impeded more in tumors (Fig 8).

The main diffusion-weighted imaging derived parameter, the ADC, has been correlated with important histologic properties, including the tumor proliferation index, tumor grade, the presence of necrosis, and tumor cell apoptosis (26,47–49). In addition, the information obtained with diffusion imaging can be quantified and displayed as parametric maps (functional diffusion map or ADC parametric response map) (50), thus enabling the spatial heterogeneity of tissues or tumors to be analyzed before and in response to treatment (Figs 9, 10). New fusion techniques and sophisticated software permit robust qualitative evaluation of diffusion-weighted imaging data (Movie E2 [online]) and quantitative analysis of ADC changes induced by therapy (Figs 11, 12) and calculation of the relative tumor volume. The drug effects most likely to be detected with diffusion-weighted imaging are those likely to alter the microenvironmental architecture (ie, apoptosis and angiolysis) (47).

As a general rule, any therapy that causes necrosis or cellular lysis will lead to increases in water diffusion in the extracellular space, with lowering of signal intensity on high *b* value images and corresponding increases in ADC values.

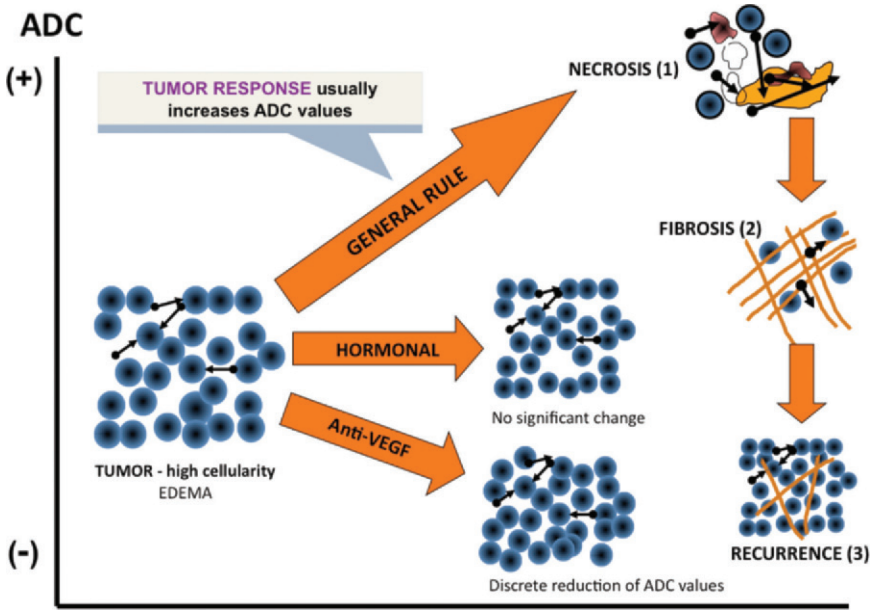

Figure 11. ADC changes after therapy. Cancer treatment induces cell death by apoptosis, necrosis, and cell lysis, which lead to an increase in the mobility of water in the tissue microenvironment. This increase in water diffusion translates to an increase in the measured tissue ADC *(1)*. In some scenarios, there may be an initial increase in ADC with a subsequent decrease that dips below the anticipated normal range *(2)*. This ADC reduction may be attributed to fibrosis or inflammatory response. However, tumor growth or disease progression can lead to further ADC reduction *(3)*. In addition, antihormonal therapy in prostate cancer and antiangiogenic therapy may not cause an initial increase in ADC values.

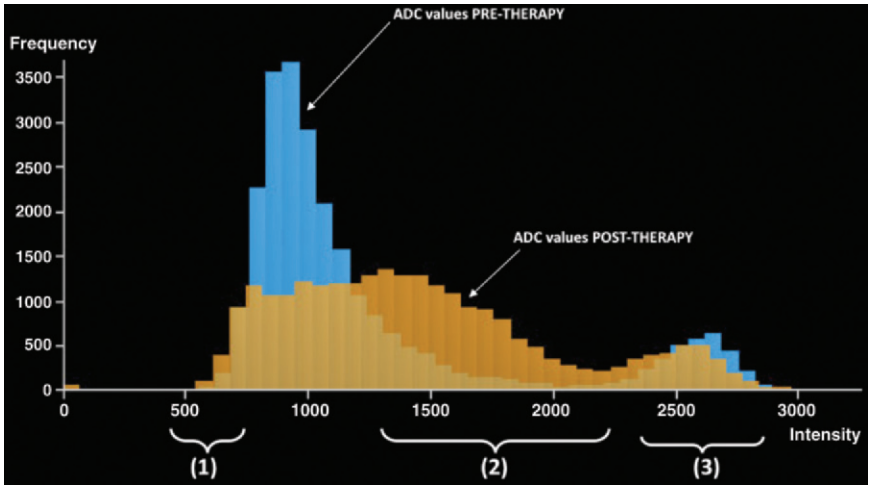

Figure 12. Multiple myeloma: bone lesion. Biologic interpretation of combined ADC histograms from all segmented voxels before (blue) and after (yellow) therapy with lenalidomide and dexamethasone. Histograms show an increase in ADC values with a greater proportion of pixels having ADC values greater than pretherapy values. A portion of the voxels *(1)* show a decrease in the ADC value; these may represent normal bone marrow after therapy. *(2)* = less cellular voxels in the tumor after therapy; *(3)* = voxels with the highest ADC values (2.5–3.0 × 10^{-3} mm^2/sec), representing necrotic areas.

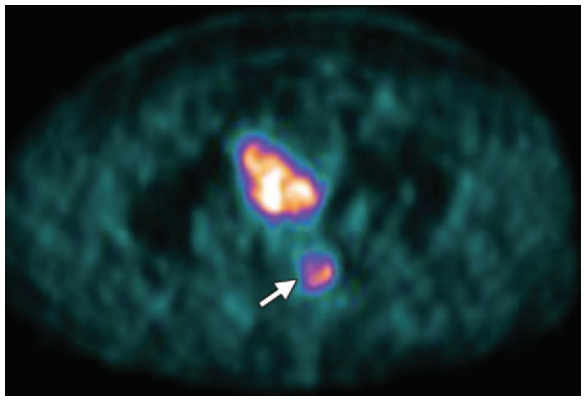

Figure 13. Rectal cancer in a 51-year-old man. Axial PET image obtained after neoadjuvant chemotherapy and radiation therapy shows a persistent high metabolic focus (arrow) in the rectal area (SUV_{max} = 5.4). Pathologic analysis of the specimen demonstrated a pT3N2 tumor.

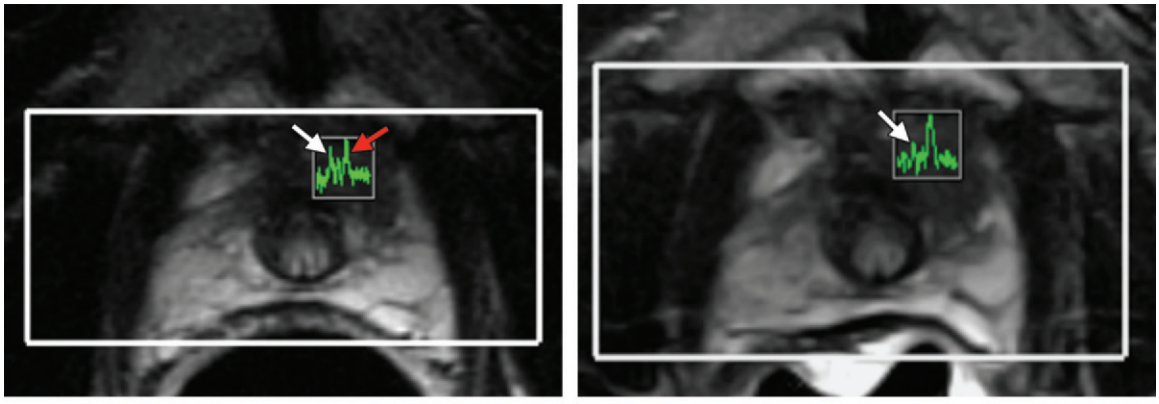

a. b.

Figure 14. MR spectroscopy of prostate cancer. **(a)** Spectrum from the voxel of interest, obtained with ^{1}H MR spectroscopy before therapy, shows a markedly elevated choline level (white arrow) that is almost equal to the citrate peak (red arrow). **(b)** Image from MR spectroscopy, obtained 3 months after hormonal therapy, shows a reduction in the choline peak (arrow). The reduction continued with increasing duration of hormone deprivation therapy.

However, it is important to consider tissue-specific responses and therapy-specific effects because there are differences in the way that diffusion-weighted imaging appearances change in response to treatment between soft-tissue tumors and bone metastases. When one is considering therapy effects on tumors, there appear to be differences in diffusion-weighted imaging findings between different therapies. For example, VDAs seem to work better in tumors with higher ADC values, but in general therapies seem to work better in more cellular tumors with lower ADC values (26,49).

Another important feature is that ADC measurements appear to be highly reproducible. Koh et al (51) evaluated measurement reproducibility of the median ADC total (calculated by using all *b* values) in a clinical trial. The coefficient of variance for ADC measurement in the body was approximately 7%; ADC total showed good measurement reproducibility, with a coefficient of repeatability expressed as a percentage of baseline average of 13.3. This means that there can be some confidence in use of the technique to detect a significant drug effect, although it may cause a relatively small percentage increase in ADC values. For example, Sun et al (52) evaluated patients with different types of tumors and showed that significant differences were seen in the percentage ADC changes between responding and nonresponding tumors ($F = 21.62$, $P < .001$).

Imaging Evaluation of Tumor Metabolism

The tumor microenvironment depends on different features including tumor vasculature and tumor cell metabolism. These features cause spatial and temporal heterogeneity in different tumor features such as oxygenation, pH, and glucose concentration (53). Two main imaging techniques allow study of tumor metabolism in vivo: PET and MR spectroscopy.

Table 6
Radiotracers Used in PET

Radiotracer	Uptake Mechanism	Indications
Oxygen 15–water	Perfusion	Tumoral perfusion
Copper 60–diacetyl-bis(N4-methylthiosemicarbazone)	Hypoxia	High sensitivity to hypoxia
Carbon 11–acetate	Synthesis of fatty acids	Genitourinary and brain imaging
^{18}F-fluoromisonidazole	Hypoxia	Imaging of the prostate and cervix
^{18}F–fluoroazomycin arabinoside	Hypoxia	Hypoxic tumors
^{18}F-fluoride	Formation of fluoroapatite	Bone metastases
^{18}F-fluorotamoxifen	Estrogen metabolism	Breast imaging
^{18}F–fluor-17-estradiol	Estrogen metabolism	Breast imaging
^{11}C- or ^{18}F-acetate	Synthesis of fatty acids	Prostate imaging
^{11}C- or ^{18}F-choline	Phospholipid synthesis	Prostate imaging
^{18}F-fluorodopa	Metabolism of amino acids	Neuroectodermal tumors
^{18}F–fluoro annexin V	Apoptosis	Tumor follow-up

Positron Emission Tomography

PET allows assessment of tissue metabolism by using radiolabeled molecules to image biologic processes in vivo. FDG is the most widely used radiotracer in PET. Increased glucose utilization in tumor cells is a well-known key cancer hallmark and has been attributed to tumor characteristics such as overexpression of membrane glucose transporters, increased hexokinase 2 activity, and decreased levels of glucose-6-phosphatase (54). FDG PET allows visualization and quantification of FDG uptake and provides a reproducible quantitative parameter of tumor glucose metabolism, the SUV (Fig 13) (Movie E3 [online]), which represents the uptake in a tumor region of interest and is based on a ratio between tracer uptake and homogeneous distribution of the tracer within the patient.

Response assessment with FDG PET can vary drastically because of a number of factors unrelated to tumor response, such as blood glucose level of the patient, change in body weight and tumor size during therapy, dose of radiotracer injected, scanner, image reconstruction algorithm, and region-of-interest selection. Unfortunately, there are no generally accepted criteria for a metabolic response in FDG PET studies, although different classifications have been proposed (Table 3), such as the European Organization for Research and Treatment of Cancer PET response criteria or the PET Response Criteria in Solid Tumors, which are based on the magnitude of the change in SUV relative to baseline (55,56). There is an increasing trend to use PET for treatment selection, response monitoring early after the start of treatment, and prediction of outcome for tumors treated with NODs (31).

FDG is not a target-specific PET tracer, and emerging new PET radiotracers may offer a clear opportunity to improve the study of many biologic features (Table 6) of great interest in tumor evaluation, such as proliferation (by using FLT PET), hypoxia (by using ^{18}F-fluoromisonidazole or ^{60}Cu–diacetyl-di-N4-methylthiosemicarbazone), or apoptosis (by using ^{18}F–fluoro annexin V). In addition, PET may allow evaluation of the expression-activity status of key tumor growth factor receptors (EGFR- or VEGFR-targeted bioprobes), which may facilitate patient selection and treatment monitoring with NODs (57,58).

MR Spectroscopy

MR spectroscopy analyzes the relative amount of chemical components within biologic tissues, allowing assessment of the molecular composition of tissues. Results are then displayed on a spectrum, which shows a series of peaks corresponding to different metabolites. Interpretation of MR spectroscopic results is based on checking the elevation of certain metabolites, such as choline, or the absence or decrease of normal metabolites that must be present in normal tissues (eg, citrate in the prostate gland or *N*-acetyl aspartate in the brain) (59,60) (Fig 14).

The most commonly used element is ^{1}H owing to its natural abundance in living organisms. ^{1}H MR spectroscopy allows study of phospholipid or glucose metabolism and cellular bioenergetics, but the main clinical use of MR spectroscopy is focused primarily on phospholipid metabolism that is associated with membrane turnover (59–61). High levels of choline, phosphomonoesters, and

Table 7
Summary of Imaging Changes in Tumors Treated with NODs

Type of Therapy	Biologic Explanation	Imaging Technique	Parameters	Change
Antiangiogenic drugs	Vascular normalization, possible necrosis	Perfusion CT*	MTT	Increased†
			BV, BF, and PSAP	Decreased†
		DCE MR imaging*	K^{trans}, k_{ep}, and v_e	Decreased†
		DSC MR imaging*	rBV, rBF	Decreased†
		DW MR imaging	ADC	Discrete transient reduction; increase if there is necrosis
		PET	SUV	No significant change or sometimes goes up (mismatch)
		MR spectroscopy	Choline peak	No significant change
Vascular disruptive agents	Necrosis, pruning of vascular network	Perfusion CT*	MTT	Increased
			BV, BF, and PSAP	Decreased
		DCE MR imaging*	K^{trans}, k_{ep}, and v_e	Decreased
			rBV, rBF	Decreased
		DW MR imaging	ADC	Increased
		MR spectroscopy	Choline peak	No data
Anti-EGFR and anti-HER2 drugs	Antiproliferative effect, induction of apoptosis	PET (FDG, FLT)*	SUV	Decreased
		Perfusion CT	BV, BF, and PSAP	Discrete reduction
		DCE MR imaging	K^{trans}, k_{ep}, and v_e	Decreased
		DW MR imaging	ADC	Increased
		MR spectroscopy	Choline peak	No data
Inhibitors of the PI3K/Akt/mTOR pathway	Antiproliferative effect, decreased vascularity	Perfusion CT*	MTT	Increased
			BV, BF, and PSAP	Decreased
		DCE MR imaging*	K^{trans}, k_{ep}, and v_e	Decreased
		PET (FDG, FLT)	SUV	Variable
NODs targeting the cKIT pathway	Change in glucose metabolism, antiproliferative effect, decreased vascularity	PET (FDG, FLT)*	SUV	Decreased
		Perfusion CT	BV, BF, and PSAP	Decreased
		DCE MR imaging	K^{trans}, k_{ep}, and v_e	Decreased
Hormonal therapy	Glandular atrophy, decreased vascularity and microvessel permeability	DCE MR imaging*	K^{trans}, k_{ep}, and v_e	Decreased
		DW MR imaging*	ADC	Variable: minimal change in prostate; increased in metastatic disease
		MR spectroscopy*	Choline peak	Decreased

Note.—BF = blood flow, BV = blood volume, DSC = dynamic susceptibility contrast, DW = diffusion-weighted, k_{ep} = rate constant, K^{trans} = transfer constant, MTT = mean transit time, PSAP = permeability–surface area product, rBF = relative blood flow, rBV = relative blood volume, v_e = leakage space fraction.
*Main imaging techniques for evaluation of response to therapy. †Mainly antipermeability effect; transient normalization phenomenon with increased flow.

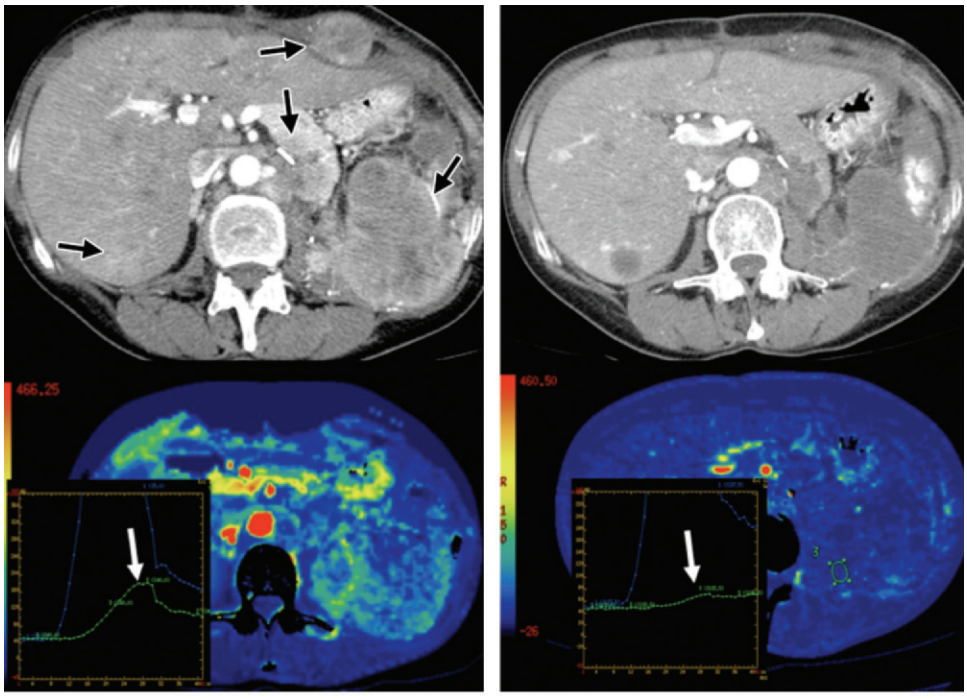

a. b.

Figure 15. Diffuse metastatic disease from renal cancer in a 58-year-old woman. Axial CT images, blood flow parametric maps, and time-attenuation curves, obtained before **(a)** and 10 days after **(b)** therapy with sunitinib (an anti-VEGF drug), show a partial response. There is disappearance of some metastatic foci (black arrows in **a**), necrotic changes in some, change in enhancement curve (white arrow), and blood flow decrease of 95% in the tumor (median blood flow, 256 vs 22 mL/min/100 mL).

phosphodiesters (breakdown products of cell membrane components) are characteristic metabolic features of cancer.

Imaging Evaluation of Tumor Proliferation

FLT is a thymidine analog that follows the salvage pathway of DNA synthesis but is not incorporated into the DNA molecule. Intracellular trapping of FLT is increased in malignant cells and correlated with cellular proliferation (57,58) and may be a more specific tracer for malignancy than FDG, since FLT PET does not show uptake in inflammatory tissues and benign tumors.

Diffusion-weighted MR imaging as a measure of cell density was discussed earlier, but a possible correlation between ADC values and proliferation index has been noted in some tumors (62).

Imaging Evaluation of Hypoxia

Tumor hypoxia is also an attractive therapeutic target (63), although hypoxia imaging is a challenge in daily practice. ^{18}F-fluoromisonidazole, ^{60}Cu–diacetyl-di-N4-methylthiosemicarbazone, and blood oxygen level–dependent MR imaging may be the leading noninvasive imaging techniques for studying tumor hypoxia (7,8). Blood oxygen level–dependent MR imaging exploits the increase in the transverse relaxation rate (R2*) of water caused by the paramagnetic effect of endogenous deoxyhemoglobin present in areas of hypoxia.

Assessment of NODs with Imaging

The use of imatinib in cKIT-expressing GISTs represents an example of personalizing molecularly targeted therapies based on biomarkers. However, different target therapies, such as EGFR agents and antiangiogenic agents, have mostly been used in unselected patient groups, and no key imaging biomarkers that predict or reflect the efficacy of these agents have been validated in clinical practice. Nevertheless, potential imaging biomarkers, such as in functional imaging for antiangiogenesis therapy, have been identified and others are under evaluation or in development.

Antiangiogenic and Antivascular Therapies

Quantitative CT and MR imaging kinetic parameters can provide insights into underlying tissue pathophysiologic processes and also allow prediction of response or monitoring of the effects of a variety of treatments (64). A number of studies have reported on use of these techniques for monitoring the effects of antiangiogenic or vascular disruptive treatments (Table 7). The effects of antiangiogenic drugs and VDAs on DCE MR imaging kinetic vascular parameters have been found to be similar, with the dominant effect of successful therapy being reductions in blood flow and permeability (Fig 15).

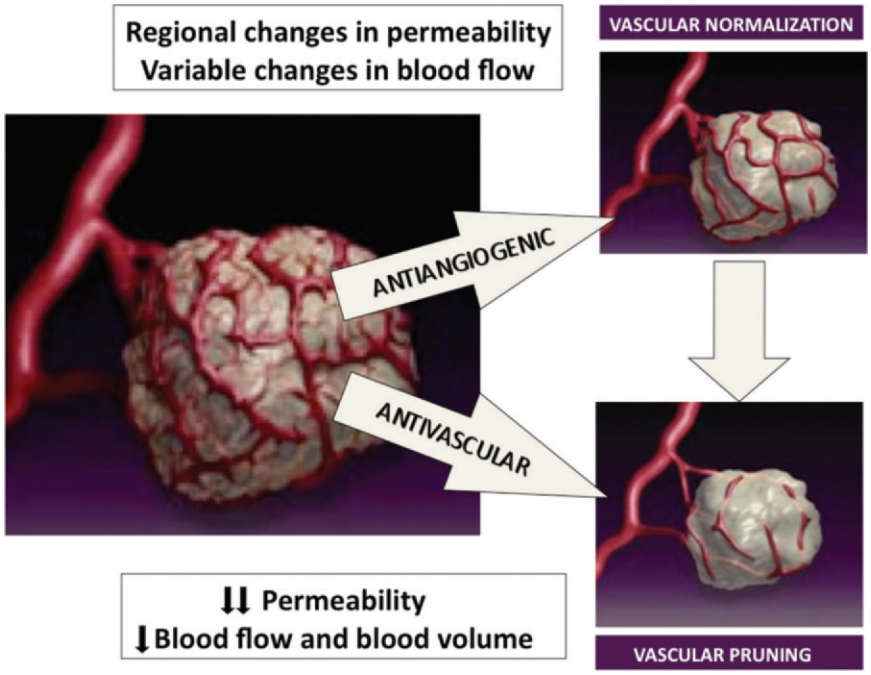

Figure 16. Mechanisms of action of antiangiogenic therapy versus VDAs. Antiangiogenic therapies initially improve both the structure and function of tumor vessels. During this normalization window, cancer cells may be more vulnerable to traditional cytotoxic therapies and novel targeted therapies.

The timing of the onset and duration of vascular changes enables the effects of antiangiogenic drugs and VDAs to be distinguished at imaging. Imaging studies of antiangiogenic drugs show that antivascular effects are not immediate, arising at least 1–2 days after drug administration. In contrast, VDAs cause rapid shutdown of the vasculature within minutes to hours of administration, with reversibility of the effects being visible in the short term (usually seen within 24–48 hours) (40,41,65).

Anti-VEGF agents can prune tumor vessels, thus killing a fraction of cancer cells, and can reduce the number of blood-circulating endothelial cells and progenitor cells. In addition, anti-VEGF agents can decrease tumor vessel permeability and interstitial fluid pressure in a process of normalization of the structure and function of tumor vasculature that can improve oxygenation and perfusion, favoring drug delivery (66,67) (Fig 16). However, in gliomas, normalization of the vascular bed involves restoration of the blood-brain barrier, thereby hampering instead of enhancing the delivery of therapeutic compounds to tumor cells (68,69) (Fig 17). Regardless of the mechanisms involved, monotherapy with bevacizumab is not curative because it cannot kill all cancer cells; in the longer term, it leads to a vasculature that is inefficient for drug delivery and to tumor relapse by means of alternative pathways for neovascularization.

Finally, there is a need to establish clear thresholds for a significant response when using quantitative DCE MR imaging or perfusion CT kinetic parameters for assessment of therapy response. It is widely recognized that reductions in K^{trans} of 30%–50% probably represent a significant change in cases of extracranial malignancies where a therapy-induced change can be inferred (66). For example, Ng et al (70) reported that the rate of reproducibility of DCE MR imaging parameters is in the range of 10%–20% and is influenced by lesion location, with the parameters being significantly more reproducible in the liver than in the lung. Goh et al (71) demonstrated that perfusion CT parameters showed low interobserver variation. In addition, changes in dynamic MR imaging and CT-based perfusion parameters such as K^{trans}, blood flow, blood volume, or permeability have been shown to occur after treatment with bevacizumab or anti-VEGFR tyrosine kinase

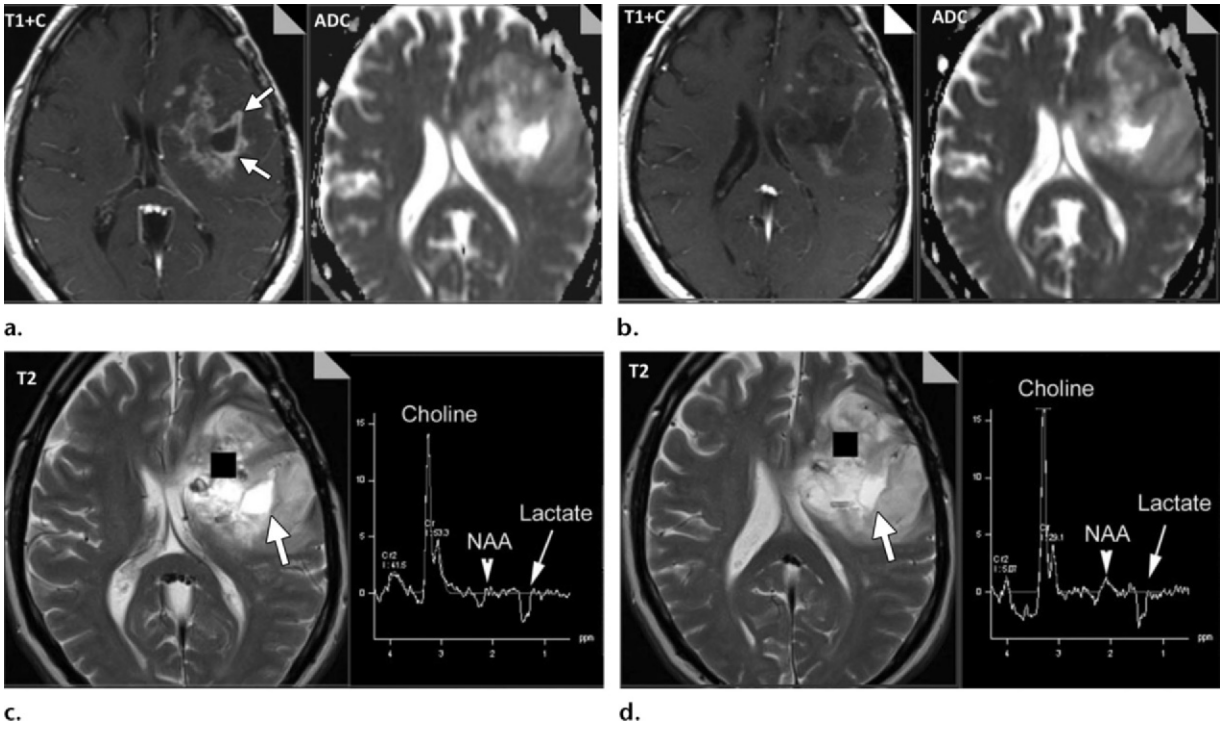

Figure 17. High-grade glioma in a 40-year-old man treated with anti-VEGF antibody therapy. **(a, b)** Contrast-enhanced T1-weighted MR images and ADC maps, obtained after 14 days **(a)** and 12 weeks **(b)** of bevacizumab therapy, show marked reduction of the rim of contrast enhancement (arrows in **a**), indicating that capillary permeability has been reduced due to vascular normalization. However, values on the ADC map have not increased, indicating absence of significant killing of tumor cells. **(c, d)** T2-weighted MR images and MR spectroscopic images, obtained after 14 days **(c)** and 12 weeks **(d)** of bevacizumab therapy, show that the tumor has increased in size and thickness by growing into the area of necrosis (large arrow). The MR spectrum (obtained from the black square on the T2-weighted image) remains unchanged, indicating that there has been no cell death. The large choline peak correlates with hypercellularity, the reduced *N*-acetyl aspartate *(NAA)* peak (arrowhead) indicates that neurons have been destroyed or displaced, and the inverted lactate peak (small arrow) is indicative of anaerobic glycolysis.

receptor inhibitors in different type of tumors. Changes in these parameters are greater than the level of reproducibility, thus potentially enabling these data to be useful for monitoring antiangiogenesis therapy and associated with improved progression-free survival and overall survival (72).

Diffusion-weighted MR imaging allows evaluation of antiangiogenesis therapy directed to the VEGF pathway. These agents cause reductions in tumor ADC values that coincide with reductions in contrast enhancement (Fig 17a, 17b). The principal explanation appears to be reduction of the lesion extravascular-extracellular space secondary to vascular normalization and lowering of vascular permeability. These reductions in ADC values are not always marked with antiangiogenesis therapy. Indeed, increased ADC is observed if there is significant tumor necrosis caused by the treatment. Similar findings of an increase in ADC values have also been noted with VDAs, which usually induce massive necrosis within tumor centers (26,73,74).

With MR spectroscopy, evaluation of response to anti-VEGF or anti-VEGFR therapy does not demonstrate significant changes in metabolites after bevacizumab therapy of brain tumors (75) (Fig 17c, 17d).

PET has also been used to evaluate drugs that interfere with the VEGFR or PDGF receptor pathways. Use of bevacizumab or sorafenib as well as a combination of these agents in several types of solid tumors usually showed no changes at FDG PET (76); however, published data seem

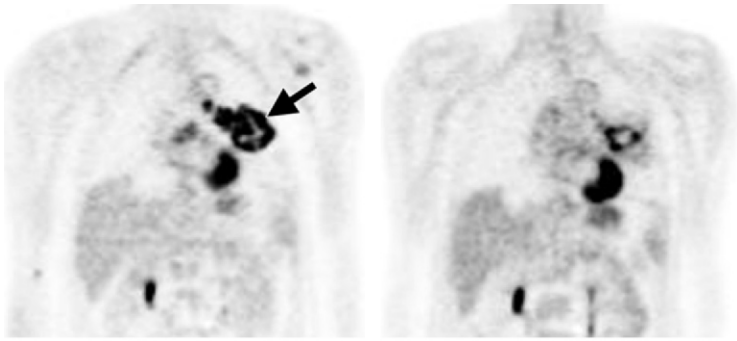

Figure 18. Lung adenocarcinoma with a mutation in exon 21 of EGFR in a 55-year-old woman with no history of smoking. PET images obtained before **(a)** and after **(b)** erlotinib anti-EGFR therapy show a partial response, with decreases in the size of the tumor (arrow in **a**) and in SUV_{max} (18.3 before therapy vs 10.2 after therapy).

to be contradictory between different series. A possible explanation could be that changes in perfusion may interfere with FDG extraction in tissues or tumors. Antiangiogenesis therapy may cause decreases in perfusion attributable to vascular pruning in the tumor or increases attributable to reduced interstitial pressure and vascular normalization. However, use of dynamic FDG studies with quantitative analysis and kinetic modeling may overcome this limitation (31). Another study suggests that FDG PET or FLT PET may not be suitable for evaluation of early markers of response to antiangiogenic agents and mTOR inhibitors in which antiangiogenic or vascular effects predominate because the method could produce false-negative results (77).

Anti-EGFR and Anti-HER2 Drugs

There is only limited experience with evaluation of anti-EGFR and anti-HER2 drugs with functional imaging. Published data suggest that FDG PET may allow early and quantitative assessment of therapeutic efficacy, thus supporting its incorporation into clinical testing of these targeted cancer drugs (31,54,57,58) (Fig 18). In patients with non–small cell lung cancer treated with erlotinib or gefitinib, an FDG PET study demonstrated increases in glucose metabolism after discontinuation of therapy, followed by decreases in SUV_{max} with reintroduction of erlotinib or gefitinib therapy (78).

However, PET may open new perspectives with use of new radiotracers such as FLT that may improve detection of early tumor response to EGFR inhibitors (79) or with development of EGFR-targeted radiotracers to improve patient selection and treatment monitoring (80). For example, FLT PET was found to allow prediction of response to EGFR inhibitors and patient outcome (positive and negative predictive values of 92.9%); a reduction in SUV_{max} of greater than 10.4% 7 days after gefitinib therapy was predictive of a RECIST response at CT 6 weeks after therapy (81). In that study, the percentage changes in SUV_{max} were significantly different between responders and nonresponders (–36.0% ± 15.4 vs 10.1% ± 19.5, $P < .001$).

Evaluation of EGFR inhibitors with perfusion techniques has been limited. In patients with nasopharyngeal cancer treated with combined therapy including cetuximab, DCE MR imaging did not show a significant change in quantitative parameters (4,82) (Fig 19). In contrast, DCE CT in patients with non–small cell lung cancer demonstrated a significant decrease in tumor blood flow after sorafenib and erlotinib therapy; early changes in tumor blood flow correlated with an objective response, and patients with a decrease in tumor perfusion greater than the median at week 6 tended to have a longer progression-free survival (7.1 months vs 5.7 months, $P = .06$) (83).

To our knowledge, there are no published articles on evaluation of anti-EGFR and anti-HER2 agents with diffusion-weighted MR imaging. However, it seems rationale to expect increases in ADC values with successful antiproliferative drug therapy.

Finally, increased understanding of the mechanics of the EGFR pathway has revealed that the efficacy of these medications seems to corre-

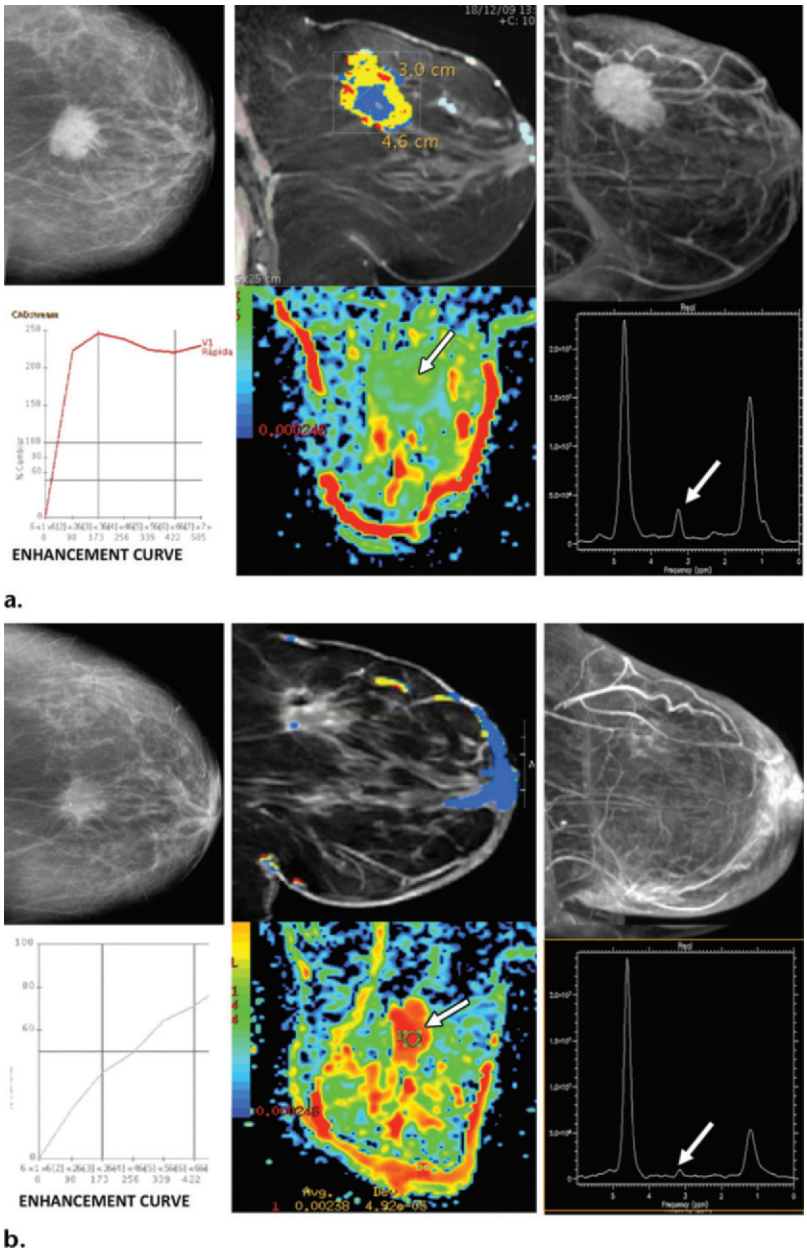

Figure 19. Invasive ductal carcinoma in a 56-year-old woman. **(a)** Pretherapy images. Top left: Mammogram shows a 5-cm mass. Top center, top right: Color-coded contrast material uptake parametric map (top center) and maximum intensity projection (MIP) image (top right) from DCE MR imaging show the enhancing mass. Bottom left: Enhancement curve for the mass shows a type III curve, which is suspicious for malignancy. Bottom center: ADC map shows a mean ADC of 0.9×10^{-3} mm^2/sec in the mass (arrow). Bottom right: Image from MR spectroscopy shows a marked choline peak (arrow). **(b)** Images obtained after chemotherapy and anti-HER2 therapy with trastuzumab. Top left: Mammogram shows the residual mass. Top center, top right: Color-coded contrast material uptake parametric map (top center) and MIP image (top right) from DCE MR imaging show changes in dynamic enhancement that are mainly secondary to conventional chemotherapy. Bottom left: Enhancement curve shows progressive enhancement, which is nonsuspicious for malignancy. Bottom center: ADC map shows a high ADC value of 2.6×10^{-3} mm^2/sec (arrow). Bottom right: Image from MR spectroscopy shows a decreased choline peak (arrow). Tumorectomy revealed fibrosis without tumor cells.

late with the presence of mutations in the EGFR gene (84) (Fig 20) (Movie E4 [online]). It is now widely accepted that specific activating mutations in EGFR allow prediction of the response of non–small cell lung cancer to these NODs. Similar findings have been demonstrated in cases of colorectal cancer and mutations in KRAS (a tyrosine kinase of the pathways activated by EGFR signaling). Recent data suggest that both cetuximab and panitumumab are effective only in the treatment of colorectal cancer with a wild-type KRAS gene; patients with tumors harboring mutations in KRAS are resistant to these two EGFR inhibitors. All of these features clearly illustrate the increasing importance of molecular biology in selection of cancer treatments.

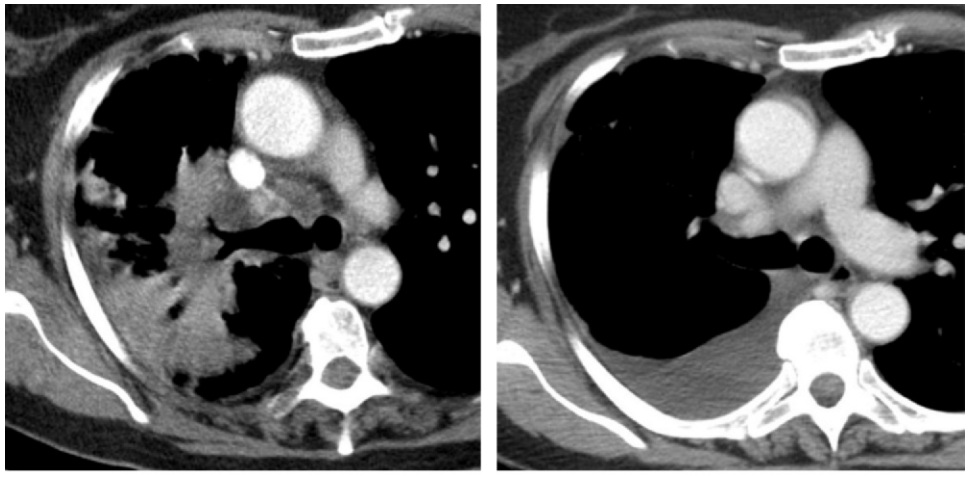

a. b.

Figure 20. Lung adenocarcinoma with a deletion in exon 19 of EGFR in a 65-year-old woman with no history of smoking. **(a)** Pretherapy axial CT image shows tumoral consolidation in the right lung. **(b)** Axial CT image obtained after erlotinib anti-EGFR therapy shows almost complete disappearance of the consolidation. Seventy-five percent of tumors that respond to EGFR-targeted tyrosine kinase receptor inhibitors contain an activating EGFR mutation. EGFR mutations are found in lung cancers (mainly adenocarcinomas) arising in nonsmokers and are more frequent in the Asian population and in women.

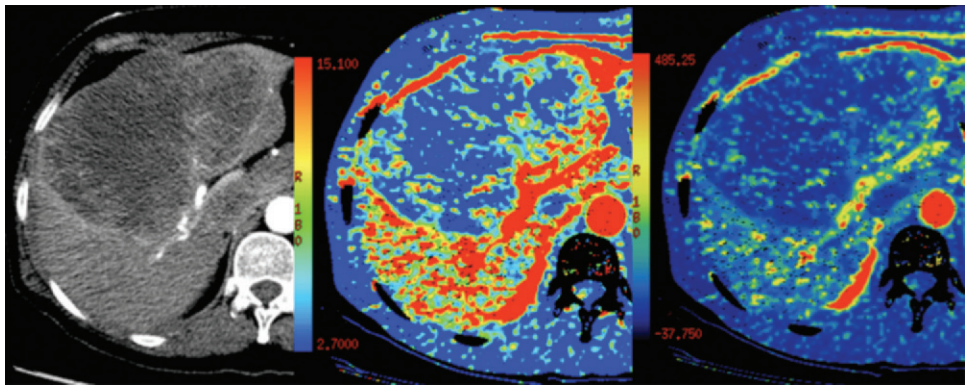

Figure 21. Liver metastasis from renal cancer after treatment with the anti-mTOR drug temsirolimus. Axial CT image (left) and parametric maps of blood volume (center) and blood flow (right) show low perfusion parameters in the metastasis.

Inhibitors of the PI3K/Akt/mTOR Pathway

Many clinical observations support targeting the downstream signaling PI3K/Akt/mTOR pathway in human cancer (16). This pathway is a convergence point for many growth stimuli (Fig 1) and, through its downstream substrates, controls cellular processes that contribute to the initiation and maintenance of key tumor processes, including tumor proliferation and metabolism. The main PI3K/Akt/mTOR pathway inhibitors are rapamycin and its analogs (everolimus and temsirolimus), which target a distal pathway component, mTOR. Activation of mTOR in response to growth, nutrient, and energy signals leads to an increase in protein synthesis, which is required for tumor development.

PET studies show decreases in metabolic activity and tumor proliferation with mTOR inhibitors, but it is not clear that an early PET response correlates with a clinical response to these drugs (77,85,86). mTOR signaling is critical in the development of many tumors, including renal cell carcinoma, in which mTOR plays a specific role in the angiogenesis pathways that are frequently upregulated via HIF. To our knowledge, no clinical

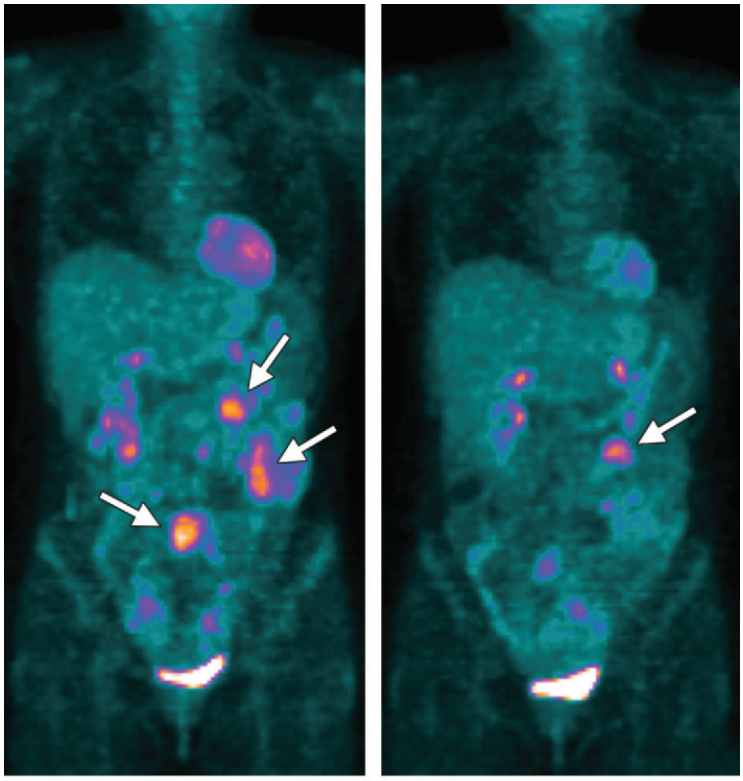

a. b.

Figure 22. GISTs in a 53-year-old woman. **(a)** Pretherapy coronal MIP PET image obtained with 374 MBq of FDG shows multiple GISTs (arrows). **(b)** PET image obtained with 400 MBq of FDG 72 hours after therapy with imatinib mesylate shows an early partial response with a decrease in tumor uptake (arrow).

studies have used DCE CT or DCE MR imaging to measure response to anti-PI3K/Akt/mTOR therapy; however, preclinical DCE MR imaging studies have shown slightly reduced tumor blood volume after 2–7 days of treatment (87) (Fig 21).

NODs Targeting the cKIT Pathway

NODs targeting the cKIT pathway have mainly focused on GISTs treated with imatinib. No other targeted agent has generated as much interest in response monitoring with FDG PET (Fig 22) (Movie E5 [online]). Many studies have found that FDG PET shows a dramatic decrease in glucose metabolism.

Criteria for therapeutic response assessment have also been established for FDG PET. The European Organization for Research and Treatment of Cancer has defined guidelines for use of FDG PET in GISTs. These guidelines state that a 25% reduction in SUV_{max} should be considered the threshold for definition of a partial response (56). This finding can be observed as early as 24 hours after the start of treatment, and an early decrease in SUV_{max} after commencement of treatment is associated with longer progression-free survival (92% vs 12% at 1 year, $P = .00107$) (88).

Diffusion-weighted MR imaging may represent a useful predictive biomarker in GISTs treated with imatinib mesylate. In a recent study, a low pretherapy ADC and marked ADC increase 1 week after therapy were associated with a good response. Tang et al (89) reported an early and statistically significant ($P < .001$) increase in ADC in patients with a good response (median ADC increase, 44.8%) but not in patients with a poor response (median ADC increase, 1.5%).

Hormonal Therapy

Hormonal therapy is a powerful therapeutic option in hormone receptor–positive breast cancer and prostate cancer. Steroid hormones are drivers of gene expression in certain cancer cells; changing the levels or activity of hormones can cause certain cancers to cease growing or even undergo cell death. Androgen deprivation shows antivascular effects in prostate cancer, with reductions in tumor blood volume and blood flow within the 1st month; changes in DCE MR imaging parameters can also be seen (90).

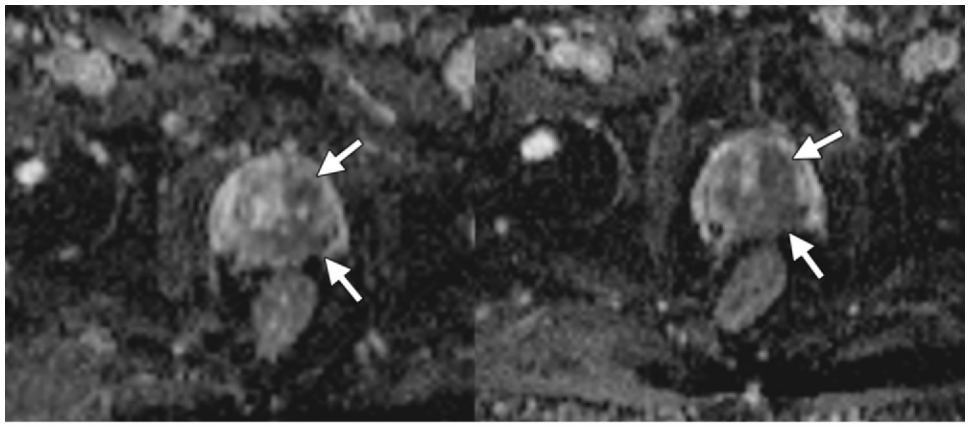

a.

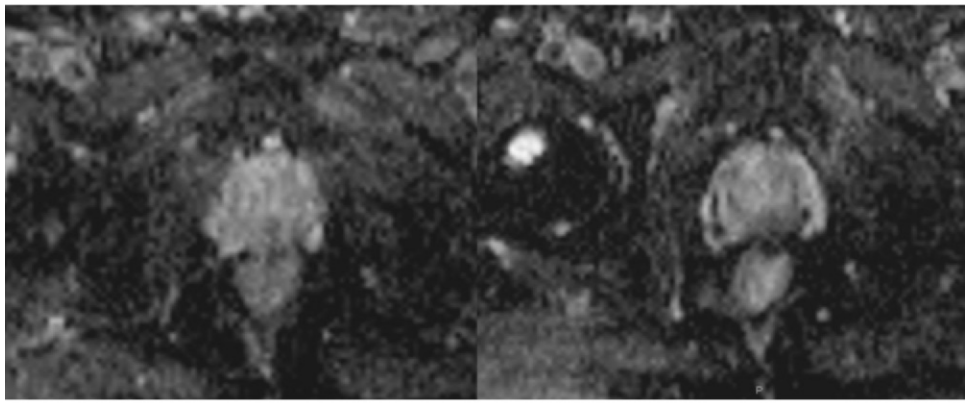

b.

Figure 23. Multifocal prostate cancer in a 68-year-old man. **(a)** ADC maps obtained before hormonal therapy show extensive areas of low ADC (mean, 0.8×10^{-3} mm^2/sec) (arrows). **(b)** ADC maps obtained 3 months after hormonal therapy show increased ADC values (mean, 1.25×10^{-3} mm^2/sec) in the areas of low ADC in **a**. This is not the usual response to hormonal therapy in prostate cancer. In general, hormonal therapy does not change ADC values in prostate cancer.

Initial data from diffusion-weighted MR imaging of patients with prostate cancer treated with hormonal therapy suggest a minimum change in prostate ADC values, although there is limited experience in this field and further studies are necessary (91) (Fig 23). ^{1}H MR spectroscopy of patients with prostate cancer treated with hormonal therapy demonstrates reductions in citrate peaks in the tumor and normal peripheral zone, a finding consistent with glandular atrophy, as well as slower loss of choline and creatine with increasing duration of hormone deprivation therapy (92) (Fig 14). In this setting, persistent elevation of choline levels can indicate ongoing active disease in the prostate gland.

FDG PET shows only limited value in evaluating response in prostate cancer, whereas tamoxifen and aromatase inhibitors produced an increase in tumor FDG uptake early after treatment in some patients with breast cancer. This increase in FDG uptake after therapy is the so-called metabolic flare and reflects a hormone-induced change in tumor metabolism. This phenomenon has been correlated with positive tumor response to hormonal therapy in breast cancer. Dehdashti et al (93) noted a higher tumor SUV in responders (SUV = 3.5 ± 2.5) than in nonresponders (SUV = 2.1 ± 1.8) (P = .0049) and longer overall survival in patients with metabolic flare (P = .0062).

Whole-body diffusion-weighted MR imaging also appears to be useful for monitoring the effect of hormonal therapy in breast cancer and prostate cancer (Fig 24). Successful treatment resulting in substantial cell killing appears to lower signal intensity on high b value images, while disease progression appears as new areas of abnormal signal intensity or changes in the extent, symmetry, and intensity of abnormalities (26).

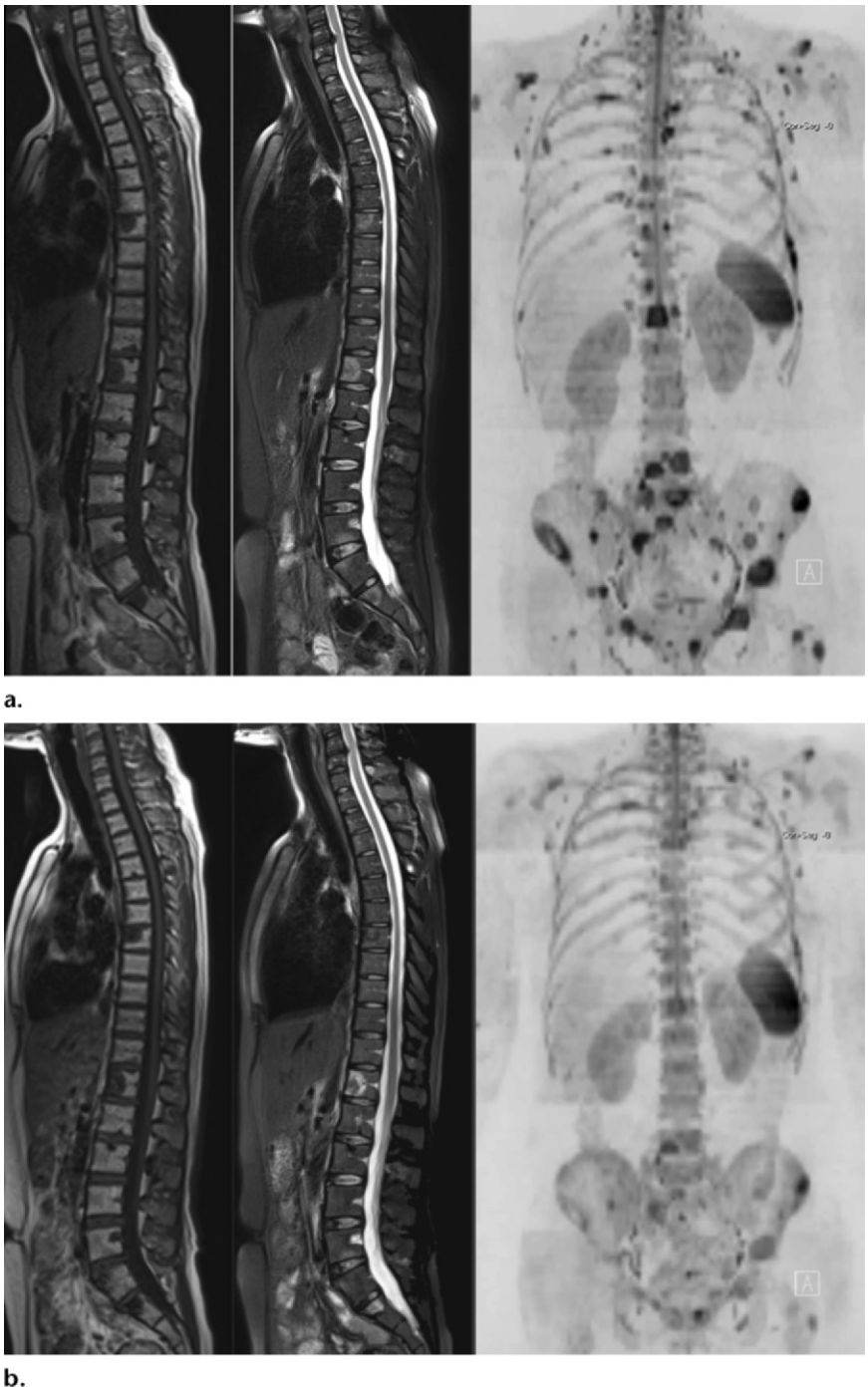

Figure 24. Treatment response of metastases at MR imaging. Sagittal T1-weighted (left) and T2-weighted (center) turbo spin-echo MR images and whole-body diffusion-weighted MR images with an inverted gray scale (b = 800 sec/mm^2) (right) show metastases before **(a)** and after **(b)** hormonal therapy with an aromatase inhibitor. The conventional MR images show no significant change after therapy, while the diffusion-weighted images show death of metastatic cells after hormonal therapy.

Aromatase inhibitors also cause bone marrow atrophy, which is observable with whole-body diffusion-weighted imaging.

New Therapeutic Agents

Currently, the capabilities of functional and molecular imaging include the ability to image gene expression, receptors, signaling pathways, apoptosis, the extracellular matrix, and hypoxia (94). On this basis, many other new therapeutic agents are under development, including HIF-1α inhibitors, matrix metalloprotease inhibitors, and integrin avb3 inhibitors. Among these, antihypoxia drugs may represent the most attractive future target, with hypoxia-specific cytotoxins appearing as the most promising hypoxia-directed agents (8,63). However, there are limited data on imaging evaluation of these agents in clinical practice (95).

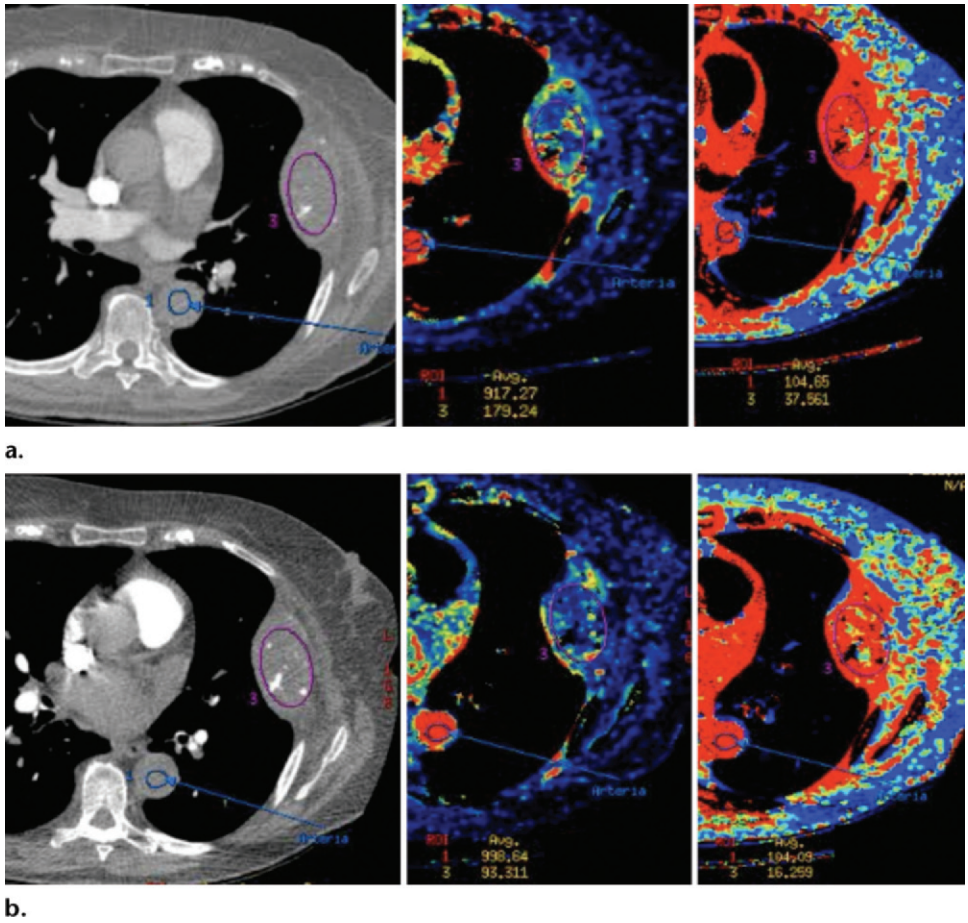

Figure 25. Bone metastases from renal cancer in a 63-year-old woman. Axial CT images (left) and parametric maps of blood flow (center) and blood volume (right), obtained before **(a)** and 15 days after **(b)** therapy with the anti-VEGF drug sunitinib, show no change in lesion size (blue circles, purple ovals). The parametric maps show a 40% decrease in blood flow and 60% decrease in blood volume, but a significant decrease in perfusion parameters that may show a correlation with clinical end points (time to progression, disease-free survival) has not been established. Future standardization of data acquisition and response criteria is required.

Future Challenges and Opportunities

Biomarkers are characteristics that may be measured objectively as indicators of normal biologic processes, pathologic changes, or pharmaceutical responses to a therapeutic intervention. Anatomic, functional, or molecular parameters detected with imaging may function as tumor response biomarkers (96). In addition, quantitative imaging biomarkers may be of assistance in drug development. In this last setting, they allow identification of therapeutic targets, guidance of dose and scheduling, and demonstration of proof of concept, proof of mechanism, and drug efficacy; they can also be early surrogate end points of benefit (97,98). However, there are several challenges that imaging needs to overcome before being used for evaluation of response biomarkers.

First, cancers are complex ecosystems that are characterized by profound spatial and temporal heterogeneity. An emerging concept states that tumors with the most heterogeneity are more readily adaptable to perturbations, such as chemotherapy, and thus have the worst prognosis (67). Tumor heterogeneity is a major feature of tumor resistance. Imaging techniques should be able to represent the functional, anatomic, and pathophysiologic features of tumor heterogeneity.

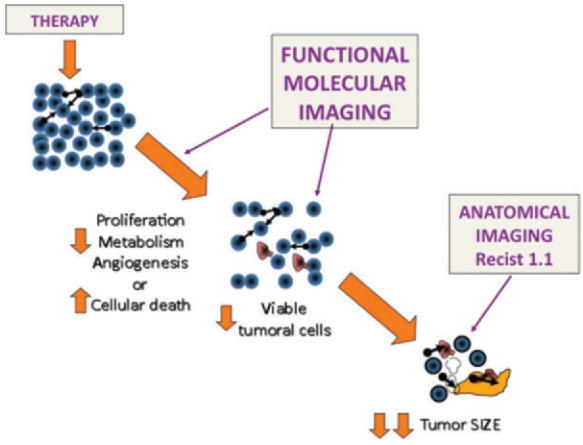

Figure 26. Functional and molecular imaging may demonstrate an early tumor response in advance of anatomic changes (decrease in size).

Second, tumor response is often differential throughout the neoplasm. Functional imaging techniques are increasingly used to provide in vivo assessment of tumor features. However, if the evaluation is of a limited volume, the results may be unrepresentative of the tumor burden. Whole-body techniques may compensate for spatial variability

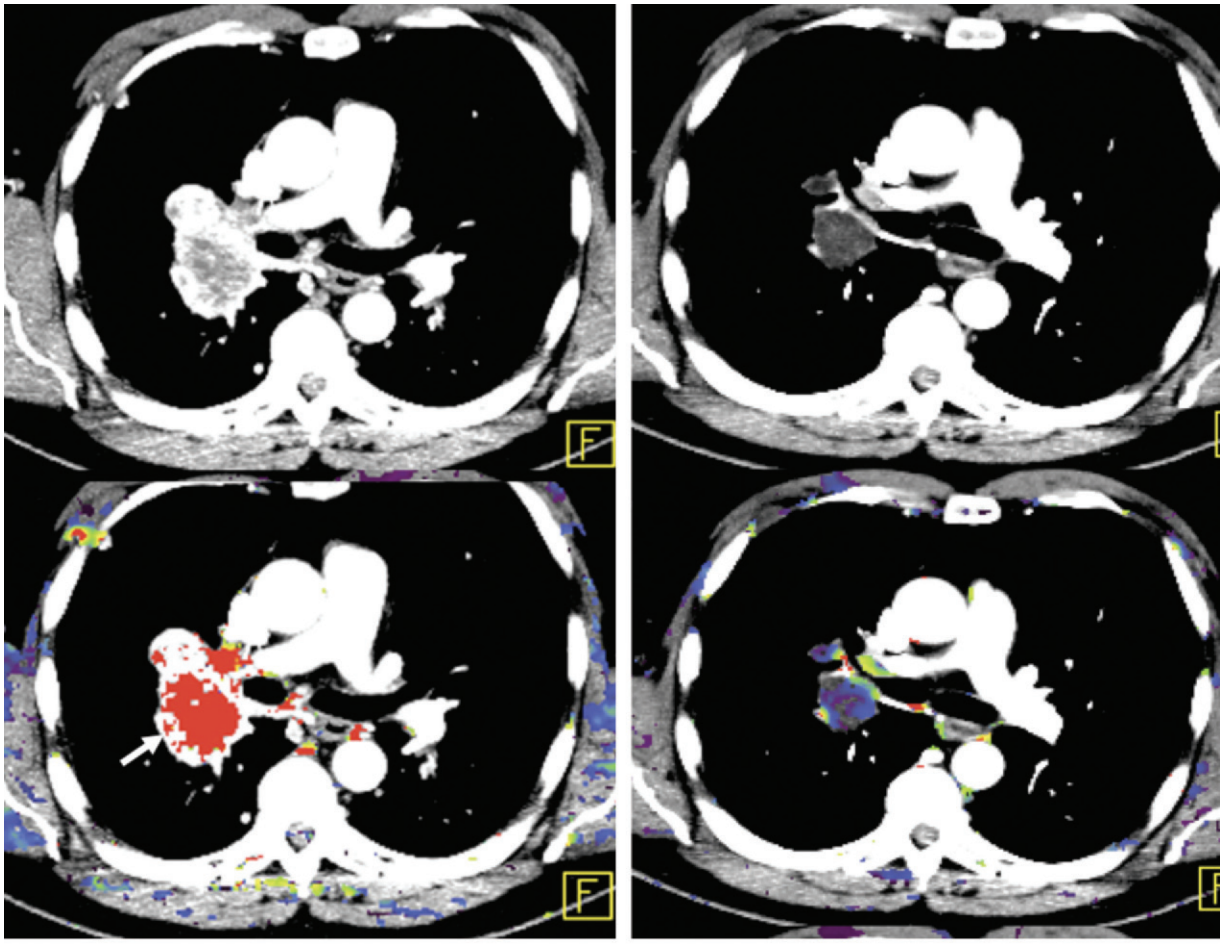

a. b.

Figure 27. Metastatic renal cancer. MIP images (top) and parametric maps of blood flow (bottom), obtained before **(a)** and 15 days after **(b)** therapy with sorafenib, show decreased blood flow in the tumor (arrow in **a**) after therapy. This feature was predictive of treatment response in renal tumors treated with the multikinase VEGFR inhibitors sorafenib and sunitinib.

and potentially improve reproducibility. Whole-body imaging (eg, whole-body PET or whole-body MR imaging) allows analysis of multiple lesions and represents a viable solution to the problem of differential response (Movie E6 [online]).

Third, quantitative parameters need to be robust and repeatable across different platforms, and data acquisition and analysis methods need to be standardized. A major challenge to widespread implementation of functional and molecular imaging techniques for evaluation of response biomarkers to cancer therapies is the lack of standard approaches to data collection and analysis. In addition, to enable use of quantitative imaging parameters for evaluation of therapy response, assessments of measurement error are needed. Estimates of measurement errors allow one to decide whether changes in imaging parameters are real and significant (Fig 25).

For example, initial data suggest that the reproducibility of the mean or median change in tumor ADC is likely to be somewhere in the range of 10%–20% in extracranial applications (26). Summary parameters such as mean and median values oversimplify data and may mask critical information about tumor heterogeneity. Alternative methods of data evaluation such as histograms (Figs 10, 12) are a viable alternative, but parametric response maps (a novel method of image analysis that uses a voxel-by-voxel approach) seem to represent the most useful method of analysis. They allow separate analysis of tumor subregions and can be applied to various functional imaging techniques such as perfusion or ADC maps (26,50).

Fourth, imaging must demonstrate an early tumor response (Fig 26). Some of these functional and molecular imaging techniques allow prediction of the success of therapy before conventional size measurements demonstrate change (Fig 27) (99). For this role, the critical question of how to

Table 8
Timing of Evaluation for Drug Effects according to the Literature

Time	Drug Target	Imaging Technique
0–6 h	Vascular disruptive agent, HIF	DCE MR imaging, DCE US, diffusion-weighted MR imaging, transverse relaxation rate MR imaging
24–48 h	VEGF inhibitor	DCE MR imaging, DCE US
24–48 h	EGFR inhibitor	FDG PET
1 wk	VEGF	DCE MR imaging, perfusion CT (transient normalization phenomenon with increasing flow after VEGF therapy)
1 wk	PI3K/Akt/mTOR inhibitor	FDG PET, perfusion CT
1 wk	EGFR	FLT PET

Table 9
Relationships between Tumor Hypoxia, Perfusion, and Glucose Metabolism and Their Possible Biologic Significance

Hypoxia	Perfusion	Glucose Metabolism	Significance
Absent	Low	Moderate	Probable low tumor aggression and low-grade neoplasm
Absent	High	High	Probable constitutive upregulation of angiogenesis and metabolism, possible moderate tumor aggression
Present	Low	Low	Necrosis
Present	Low	Moderate	Failure of adaptation to hypoxia, probable tumor aggression, probable moderate treatment resistance
Present	Low	High	Adaptation to hypoxia, high tumor aggression, treatment resistance

determine the exact timing of imaging to match the expected action of the drug must be clarified. The available data on the optimal time for imaging according to the class of therapeutic agent are still preliminary (Table 8) (41,49,58).

Fifth, functional and molecular imaging must play a role in establishing a prognostic for tumor response. For this role, several published studies have suggested that in certain tumors, baseline characteristics such as a high ADC, low K^{trans}, or high SUV may represent poor prognostic factors for response to treatment with both cytotoxic chemotherapy and targeted agents (26,27,41,55,56,58).

Finally, the limitations of individual technologies must be minimized. To this end, the simultaneous use of two or more techniques to achieve multiplexed or multiparametric imaging is a promising approach (99–101). Currently, it appears clear that an adequate understanding of tumor hallmarks and improved accuracy in imaging characterization of tumor phenotype and microenvironment characteristics represent mandatory elements in evaluating tumor response to NODs.

Teaching Point

By combining data on tumor perfusion and vascularity, cellular density and necrosis, tumor metabolism, and degree of hypoxia together with the receptor expression for the intended target, an "imaging phenotype" of the tumor can be created (Table 9) and one may begin to truly understand which cellular processes are affected by therapy in vivo (Fig 28). The multiparametric approach is being used for depiction of biologic features, lesion characterization, radiation therapy planning, and improved understanding of the biologic effects of therapies.

Multiplexed evaluation uses different strategies such as combination of multiple modalities (eg, PET and CT or PET and MR imaging) or collection of multiple signals. (MR imaging may offer the greatest ability to harness differences

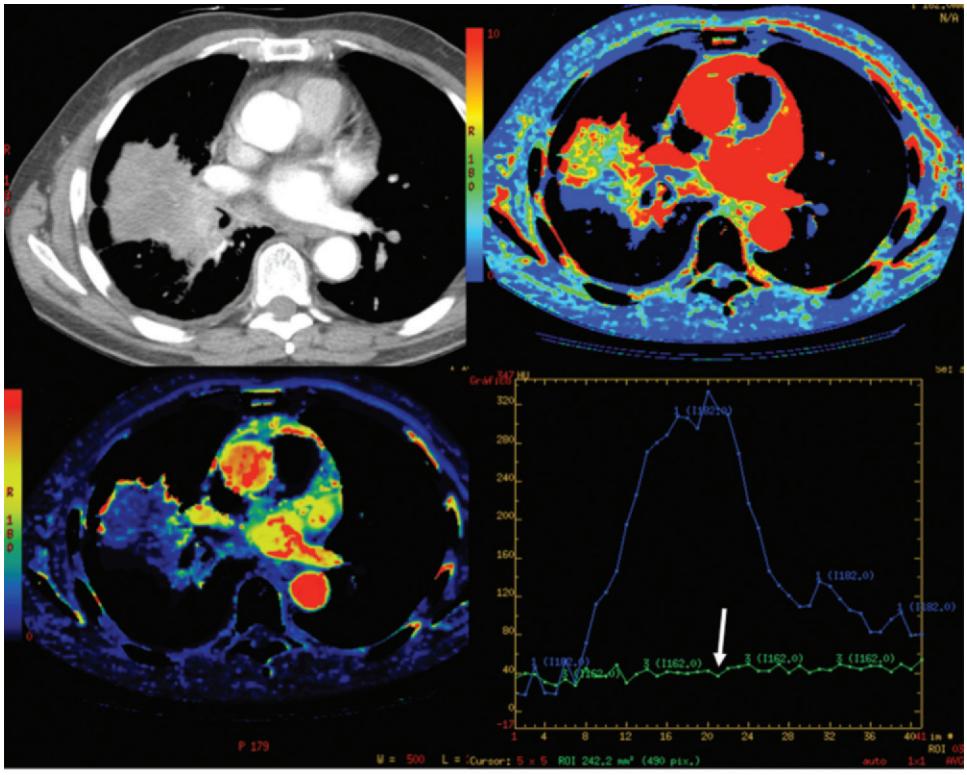

a.

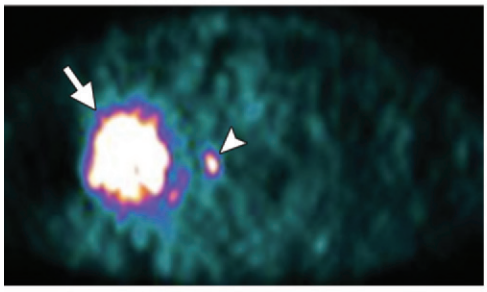

b.

Figure 28. Perfusion CT and PET of lung cancer in a 57-year-old man. **(a)** Axial CT image (top left), parametric maps of blood volume (top right) and blood flow (bottom left), and time-attenuation curve (bottom right [arrow]) show a large lung tumor with very poor perfusion. **(b)** PET image shows that the tumor (arrow) has very intense FDG uptake (SUV_{max} = 26.4) with metastatic involvement of a mediastinal lymph node (arrowhead). Balance between tumor blood flow and metabolism will be an important indicator of its biologic status. This tumor shows an aggressive phenotype with extensive regional areas of mismatch between vascularity and metabolism.

in molecular composition by collecting multiple signals: for instance, signals from T1- and T2-weighted imaging, MR spectroscopy, diffusion-weighted imaging, and DCE imaging [Fig 19].) By using this approach, anatomic, molecular, cellular, and functional imaging data may be obtained simultaneously.

Discordant results can be biologically meaningful. Thus, the balance between tumor blood flow and metabolism will be an important indicator of the biologic status of a tumor and thus the likely progression of the tumor and its response to treatment (102). Currently, integration of multidimensional imaging datasets represents a major challenge. In the future, computer platforms will need to be able to coregister and integrate multiple data analyses to follow changes in response to therapy (Fig 29).

However, important efforts in qualification and standardization need to be achieved before acceptance of some of these functional and molecular imaging biomarkers as surrogate end points. Imaging data must be correlated with clinical end points, and functional and molecular imaging techniques must be validated for every tumor and therapy. In addition, new elements such as multidrug resistance must be integrated into imaging evaluation of tumor response (103).

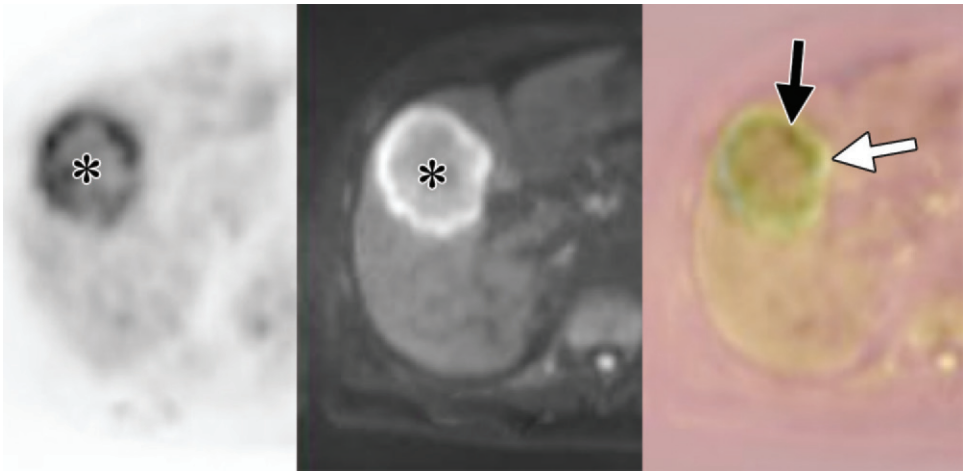

Figure 29. Fusion PET–MR imaging of a liver metastasis from colorectal cancer in a 56-year-old man. FDG PET image (left), diffusion-weighted MR image (b = 500 sec/mm^2) (center), and fused image produced with fusion software (right) show heterogeneous distribution of metabolism and cellularity in the tumor. The area of higher FDG uptake (dark area on PET image, black arrow in fused image) and the area of higher cellular density (bright area on diffusion-weighted image, white arrow in fused image) are indicative of a mismatch between metabolism and cellularity. FDG uptake is greatest at the edge of the necrotic central area (*), a finding possibly related to upregulated glucose transporters (Glut-1) secondary to hypoxic stress. The area of higher cellular density (white arrow in fused image) demonstrates FDG uptake similar to that of the normal liver.

Finally, with the use of complex multitargeted therapies, the anticipated effects on functional and molecular imaging measurements become more difficult to predict.

Conclusions

Our understanding of the complexity of cancer hallmarks and their modification by anticancer therapy is still rudimentary. We lack an integrated view and understanding of the overall effects of targeted therapies on tumor characteristics such as perfusion, glycolysis, hypoxia, and cellularity. New functional and molecular imaging techniques offer insight into these tumor hallmarks, and these imaging features should allow us to answer questions about drug development or response evaluation such as assessment and definition of response, early prediction of clinical outcome, and identification of therapeutic targets for selecting patients for a given therapy.

However, most of these techniques are still in development. Although there is accumulating evidence about the biologic meaning of the various imaging parameters, there is an imperative need for rigorous, standardized methodology in both data acquisition and analysis. The value of these imaging techniques should be demonstrated in different situations because the extent and duration of tumor changes induced by therapy depend on the type of treatment administered, lesion location, tumor type, and the timing of imaging with respect to the treatment.

In the future, by combining existing functional and molecular imaging modalities and taking new innovations from the bench to the clinic, the goals of characterization of tumor hallmarks and the tumor microenvironment, monitoring of therapy response, and improved treatment will be achieved.

***Disclosures of Potential Conflicts of Interest.*—A.R.P.:** *Related financial activities:* none. *Other financial activities:* consultant and speaker for Siemens Healthcare. **J.C.V.:** *Related financial activities:* none. *Other financial activities:* speaker for Bayer; royalties from Springer. **V.J.G.:** *Related financial activities:* none. *Other financial activities:* consultant for Siemens Healthcare and GE Healthcare.

References

1. Hanahan D, Weinberg RA. Hallmarks of cancer: the next generation. Cell 2011;144(5):646–674.
2. Hait WN, Hambley TW. Targeted cancer therapeutics. Cancer Res 2009;69(4):1263–1267; discussion 1267.
3. Seufferlein T, Ahn J, Krndija D, Lother U, Adler G, von Wichert G. Tumor biology and cancer therapy: an evolving relationship. Cell Commun Signal 2009; 7:19.
4. Desar IM, van Herpen CM, van Laarhoven HW, Barentsz JO, Oyen WJ, van der Graaf WT. Beyond RECIST: molecular and functional imaging techniques for evaluation of response to targeted therapy. Cancer Treat Rev 2009;35(4):309–321.
5. Kerbel RS. Tumor angiogenesis. N Engl J Med 2008;358(19):2039–2049.

6. Sullivan LA, Brekken RA. The VEGF family in cancer and antibody-based strategies for their inhibition. MAbs 2010;2(2):165–175.
7. Tatum JL, Kelloff GJ, Gillies RJ, et al. Hypoxia: importance in tumor biology, noninvasive measurement by imaging, and value of its measurement in the management of cancer therapy. Int J Radiat Biol 2006;82(10):699–757.
8. Padhani AR, Krohn KA, Lewis JS, Alber M. Imaging oxygenation of human tumours. Eur Radiol 2007;17(4):861–872.
9. Hinnen P, Eskens FA. Vascular disrupting agents in clinical development. Br J Cancer 2007;96(8): 1159–1165.
10. Ferrara N. Vascular endothelial growth factor as a target for anticancer therapy. Oncologist 2004;9 (suppl 1):2–10.
11. Semenza GL. A new weapon for attacking tumor blood vessels. N Engl J Med 2008;358(19):2066–2067.
12. Ciardiello F, Tortora G. EGFR antagonists in cancer treatment. N Engl J Med 2008;358(11): 1160–1174.
13. Hudis CA. Trastuzumab: mechanism of action and use in clinical practice. N Engl J Med 2007;357(1): 39–51.
14. Jones KL, Buzdar AU. Evolving novel anti-HER2 strategies. Lancet Oncol 2009;10(12):1179–1187.
15. Yuan R, Kay A, Berg WJ, Lebwohl D. Targeting tumorigenesis: development and use of mTOR inhibitors in cancer therapy. J Hematol Oncol 2009;2:45.
16. LoPiccolo J, Blumenthal GM, Bernstein WB, Dennis PA. Targeting the PI3K/Akt/mTOR pathway: effective combinations and clinical considerations. Drug Resist Updat 2008;11(1-2):32–50.
17. Sleijfer S, Wiemer E, Verweij J. Drug Insight: gastrointestinal stromal tumors (GIST)—the solid tumor model for cancer-specific treatment. Nat Clin Pract Oncol 2008;5(2):102–111.
18. El Saghir NS, Tfayli A, Hatoum HA, Nachef Z, Dinh P, Awada A. Treatment of metastatic breast cancer: state-of-the-art, subtypes and perspectives. Crit Rev Oncol Hematol 2011 Feb 16. [Epub ahead of print]
19. Mottet N, Bellmunt J, Bolla M, et al. EAU guidelines on prostate cancer. II: Treatment of advanced, relapsing, and castration-resistant prostate cancer. Eur Urol 2011;59(4):572–583.
20. Suzuki C, Jacobsson H, Hatschek T, et al. Radiologic measurements of tumor response to treatment: practical approaches and limitations. RadioGraphics 2008;28(2):329–344.
21. Eisenhauer EA, Therasse P, Bogaerts J, et al. New response evaluation criteria in solid tumours: revised RECIST guideline (version 1.1). Eur J Cancer 2009;45(2):228–247.
22. Nishino M, Jagannathan JP, Ramaiya NH, Van den Abbeele AD. Revised RECIST guideline version 1.1: what oncologists want to know and what radiologists need to know. AJR Am J Roentgenol 2010; 195(2):281–289.
23. Tuma RS. Sometimes size doesn't matter: reevaluating RECIST and tumor response rate endpoints. J Natl Cancer Inst 2006;98(18):1272–1274.
24. Marcus CD, Ladam-Marcus V, Cucu C, Bouché O, Lucas L, Hoeffel C. Imaging techniques to evaluate the response to treatment in oncology: current standards and perspectives. Crit Rev Oncol Hematol 2009;72(3):217–238.
25. Benjamin RS, Choi H, Macapinlac HA, et al. We should desist using RECIST, at least in GIST. J Clin Oncol 2007;25(13):1760–1764.
26. Padhani AR, Koh DM. Diffusion MR imaging for monitoring of treatment response. Magn Reson Imaging Clin N Am 2011;19(1):181–209.
27. O'Connor JP, Jackson A, Asselin MC, Buckley DL, Parker GJ, Jayson GC. Quantitative imaging biomarkers in the clinical development of targeted therapeutics: current and future perspectives. Lancet Oncol 2008;9(8):766–776.
28. Stephen RM, Gillies RJ. Promise and progress for functional and molecular imaging of response to targeted therapies. Pharm Res 2007;24(6):1172–1185.
29. Pysz MA, Gambhir SS, Willmann JK. Molecular imaging: current status and emerging strategies. Clin Radiol 2010;65(7):500–516.
30. Gallagher FA. An introduction to functional and molecular imaging with MRI. Clin Radiol 2010;65 (7):557–566.
31. Contractor KB, Aboagye EO. Monitoring predominantly cytostatic treatment response with 18F-FDG PET. J Nucl Med 2009;50(Suppl 1):97S–105S.
32. Chun YS, Vauthey JN, Boonsirikamchai P, et al. Association of computed tomography morphologic criteria with pathologic response and survival in patients treated with bevacizumab for colorectal liver metastases. JAMA 2009;302(21):2338–2344.
33. Smith AD, Shah SN, Rini BI, Lieber ML, Remer EM. Morphology, attenuation, size, and structure (MASS) criteria: assessing response and predicting clinical outcome in metastatic renal cell carcinoma on antiangiogenic targeted therapy. AJR Am J Roentgenol 2010;194(6):1470–1478.
34. Gillies RJ, Anderson AR, Gatenby RA, Morse DL. The biology underlying molecular imaging in oncology: from genome to anatome and back again. Clin Radiol 2010;65(7):517–521.
35. Bayouth JE, Casavant TL, Graham MM, Sonka M, Muruganandham M, Buatti JM. Image-based biomarkers in clinical practice. Semin Radiat Oncol 2011;21(2):157–166.
36. Atri M. New technologies and directed agents for applications of cancer imaging. J Clin Oncol 2006; 24(20):3299–3308.
37. Turkbey B, Kobayashi H, Ogawa M, Bernardo M, Choyke PL. Imaging of tumor angiogenesis: functional or targeted? AJR Am J Roentgenol 2009;193 (2):304–313.
38. Jeswani T, Padhani AR. Imaging tumour angiogenesis. Cancer Imaging 2005;5:131–138.
39. Padhani AR, Leach MO. Antivascular cancer treatments: functional assessments by dynamic contrast-enhanced magnetic resonance imaging. Abdom Imaging 2005;30(3):324–341.
40. Leach MO, Brindle KM, Evelhoch JL, et al. Assessment of antiangiogenic and antivascular therapeutics using MRI: recommendations for appropriate methodology for clinical trials. Br J Radiol 2003;76(spec no 1):S87–S91.
41. Zweifel M, Padhani AR. Perfusion MRI in the early clinical development of antivascular drugs: decorations or decision making tools? Eur J Nucl Med Mol Imaging 2010;37(suppl 1):S164–S182.
42. Petralia G, Bonello L, Viotti S, Preda L, d'Andrea G, Bellomi M. CT perfusion in oncology: how to do it. Cancer Imaging 2010;10:8–19.

43. Miles KA. Molecular imaging with dynamic contrast-enhanced computed tomography. Clin Radiol 2010;65(7):549–556.
44. Deshpande N, Pysz MA, Willmann JK. Molecular ultrasound assessment of tumor angiogenesis. Angiogenesis 2010;13(2):175–188.
45. Nagy JA, Chang SH, Dvorak AM, Dvorak HF. Why are tumour blood vessels abnormal and why is it important to know? Br J Cancer 2009;100(6): 865–869.
46. Goh V, Padhani AR. Imaging tumor angiogenesis: functional assessment using MDCT or MRI? Abdom Imaging 2006;31(2):194–199.
47. Padhani AR, Liu G, Koh DM, et al. Diffusion-weighted magnetic resonance imaging as a cancer biomarker: consensus and recommendations. Neoplasia 2009;11(2):102–125.
48. Patterson DM, Padhani AR, Collins DJ. Technology insight: water diffusion MRI—a potential new biomarker of response to cancer therapy. Nat Clin Pract Oncol 2008;5(4):220–233.
49. Afaq A, Andreou A, Koh DM. Diffusion-weighted magnetic resonance imaging for tumour response assessment: why, when and how? Cancer Imaging 2010;10(spec no A):S179–S188.
50. Moffat BA, Chenevert TL, Meyer CR, et al. The functional diffusion map: an imaging biomarker for the early prediction of cancer treatment outcome. Neoplasia 2006;8(4):259–267.
51. Koh DM, Blackledge M, Collins DJ, et al. Reproducibility and changes in the apparent diffusion coefficients of solid tumours treated with combretastatin A4 phosphate and bevacizumab in a two-centre phase I clinical trial. Eur Radiol 2009;19 (11):2728–2738.
52. Sun YS, Cui Y, Tang L, et al. Early evaluation of cancer response by a new functional biomarker: apparent diffusion coefficient. AJR Am J Roentgenol 2011;197(1):W23–W29.
53. Cairns RA, Harris IS, Mak TW. Regulation of cancer cell metabolism. Nat Rev Cancer 2011;11(2): 85–95.
54. Patel CN, Goldstone AR, Chowdhury FU, Scarsbrook AF. FDG PET/CT in oncology: "raising the bar." Clin Radiol 2010;65(7):522–535.
55. Wahl RL, Jacene H, Kasamon Y, Lodge MA. From RECIST to PERCIST: evolving considerations for PET response criteria in solid tumors. J Nucl Med 2009;50(suppl 1):122S–150S.
56. Young H, Baum R, Cremerius U, et al. Measurement of clinical and subclinical tumour response using [18F]-fluorodeoxyglucose and positron emission tomography: review and 1999 EORTC recommendations. European Organization for Research and Treatment of Cancer (EORTC) PET Study Group. Eur J Cancer 1999;35(13):1773–1782.
57. Nanni C, Fantini L, Nicolini S, Fanti S. Non FDG PET. Clin Radiol 2010;65(7):536–548.
58. Bussink J, Kaanders JH, van der Graaf WT, Oyen WJ. PET-CT for radiotherapy treatment planning and response monitoring in solid tumors. Nat Rev Clin Oncol 2011;8(4):233–242.
59. Kwock L, Smith JK, Castillo M, et al. Clinical role of proton magnetic resonance spectroscopy in oncology: brain, breast, and prostate cancer. Lancet Oncol 2006;7(10):859–868.
60. Pinker K, Stadlbauer A, Bogner W, Gruber S, Helbich TH. Molecular imaging of cancer: MR spectroscopy and beyond. Eur J Radiol 2010 May 27. [Epub ahead of print]
61. Podo F, Canevari S, Canese R, Pisanu ME, Ricci A, Iorio E. MR evaluation of response to targeted treatment in cancer cells. NMR Biomed 2011;24 (6):648–672.
62. Wang XZ, Wang B, Gao ZQ, et al. Diffusion-weighted imaging of prostate cancer: correlation between apparent diffusion coefficient values and tumor proliferation. J Magn Reson Imaging 2009; 29(6):1360–1366.
63. Denny WA. Hypoxia-activated prodrugs in cancer therapy: progress to the clinic. Future Oncol 2010; 6(3):419–428.
64. Harry VN, Semple SI, Parkin DE, Gilbert FJ. Use of new imaging techniques to predict tumour response to therapy. Lancet Oncol 2010;11(1): 92–102.
65. Galbraith SM, Maxwell RJ, Lodge MA, et al. Combretastatin A4 phosphate has tumor antivascular activity in rat and man as demonstrated by dynamic magnetic resonance imaging. J Clin Oncol 2003;21(15):2831–2842.
66. Jackson A, O'Connor JP, Parker GJ, Jayson GC. Imaging tumor vascular heterogeneity and angiogenesis using dynamic contrast-enhanced magnetic resonance imaging. Clin Cancer Res 2007;13 (12):3449–3459.
67. Jain RK. Normalization of tumor vasculature: an emerging concept in antiangiogenic therapy. Science 2005;307(5706):58–62.
68. Jain RK, Duda DG, Clark JW, Loeffler JS. Lessons from phase III clinical trials on anti-VEGF therapy for cancer. Nat Clin Pract Oncol 2006;3(1):24–40.
69. Claes A, Wesseling P, Jeuken J, Maass C, Heerschap A, Leenders WP. Antiangiogenic compounds interfere with chemotherapy of brain tumors due to vessel normalization. Mol Cancer Ther 2008;7(1): 71–78.
70. Ng CS, Raunig DL, Jackson EF, et al. Reproducibility of perfusion parameters in dynamic contrast-enhanced MRI of lung and liver tumors: effect on estimates of patient sample size in clinical trials and on individual patient responses. AJR Am J Roentgenol 2010;194(2):W134–W140.
71. Goh V, Halligan S, Bartram CI. Quantitative tumor perfusion assessment with multidetector CT: are measurements from two commercial software packages interchangeable? Radiology 2007;242(3): 777–782.
72. Jain RK, Duda DG, Willett CG, et al. Biomarkers of response and resistance to antiangiogenic therapy. Nat Rev Clin Oncol 2009;6(6):327–338.
73. Sorensen AG, Batchelor TT, Wen PY, Zhang WT, Jain RK. Response criteria for glioma. Nat Clin Pract Oncol 2008;5(11):634–644.
74. Rieger J, Bähr O, Ronellenfitsch MW, Steinbach J, Hattingen E. Bevacizumab-induced diffusion restriction in patients with glioma: tumor progression or surrogate marker of hypoxia? J Clin Oncol 2010;28(27):e477; author reply e478.

75. Beloueche-Babari M, Chung YL, Al-Saffar NM, Falck-Miniotis M, Leach MO. Metabolic assessment of the action of targeted cancer therapeutics using magnetic resonance spectroscopy. Br J Cancer 2010;102(1):1–7.
76. Azad NS, Annunziata C, Barrett T, et al. Dual targeting of vascular endothelial growth factor (VEGF) with sorafenib and bevacizumab: clinical and translational results [abstr]. J Clin Oncol 2007;25(18 suppl):3542.
77. Honer M, Ebenhan T, Allegrini PR, et al. Antiangiogenic/vascular effects of the mTOR inhibitor everolimus are not detectable by FDG/FLT-PET. Transl Oncol 2010;3(4):264–275.
78. Riely GJ, Kris MG, Zhao B, et al. Prospective assessment of discontinuation and reinitiation of erlotinib or gefitinib in patients with acquired resistance to erlotinib or gefitinib followed by the addition of everolimus. Clin Cancer Res 2007;13(17):5150–5155.
79. Atkinson DM, Clarke MJ, Mladek AC, et al. Using fluorodeoxythymidine to monitor anti-EGFR inhibitor therapy in squamous cell carcinoma xenografts. Head Neck 2008;30(6):790–799.
80. Mishani E, Abourbeh G. Cancer molecular imaging: radionuclide-based biomarkers of the epidermal growth factor receptor (EGFR). Curr Top Med Chem 2007;7(18):1755–1772.
81. Sohn HJ, Yang YJ, Ryu JS, et al. [18F]Fluorothymidine positron emission tomography before and 7 days after gefitinib treatment predicts response in patients with advanced adenocarcinoma of the lung. Clin Cancer Res 2008;14(22):7423–7429.
82. Ma BB, Leung SF, Kam MK, et al. A phase II study of concurrent cetuximab-cisplatin and intensity-modulated radiation therapy (IMRT) in locoregionally advanced nasopharyngeal carcinoma (NPC) with correlation using dynamic contrast-enhanced magnetic resonance imaging (DCE-MRI) [abstr]. J Clin Oncol 2008;26(Suppl):6055.
83. Lind JS, Meijerink MR, Dingemans AM, et al. Dynamic contrast-enhanced CT in patients treated with sorafenib and erlotinib for non-small cell lung cancer: a new method of monitoring treatment? Eur Radiol 2010;20(12):2890–2898.
84. Tufman A, Huber RM. Biological markers in lung cancer: a clinician's perspective. Cancer Biomark 2010;6(3-4):123–135.
85. Ma WW, Jacene H, Song D, et al. [18F]fluorodeoxyglucose positron emission tomography correlates with Akt pathway activity but is not predictive of clinical outcome during mTOR inhibitor therapy. J Clin Oncol 2009;27(16):2697–2704.
86. Aide N, Kinross K, Cullinane C, et al. 18F-FLT PET as a surrogate marker of drug efficacy during mTOR inhibition by everolimus in a preclinical cisplatin-resistant ovarian tumor model. J Nucl Med 2010;51(10):1559–1564.
87. Lane HA, Wood JM, McSheehy PM, et al. mTOR inhibitor RAD001 (everolimus) has antiangiogenic/vascular properties distinct from a VEGFR tyrosine kinase inhibitor. Clin Cancer Res 2009;15(5):1612–1622.
88. Stroobants S, Goeminne J, Seegers M, et al. 18FDG-positron emission tomography for the early prediction of response in advanced soft tissue sarcoma treated with imatinib mesylate (Glivec). Eur J Cancer 2003;39(14):2012–2020.
89. Tang L, Zhang XP, Sun YS, et al. Gastrointestinal stromal tumors treated with imatinib mesylate: apparent diffusion coefficient in the evaluation of therapy response in patients. Radiology 2011;258(3):729–738.
90. Alonzi R, Padhani AR, Taylor NJ, et al. Antivascular effects of neoadjuvant androgen deprivation for prostate cancer: an in vivo human study using susceptibility and relaxivity dynamic MRI. Int J Radiat Oncol Biol Phys 2011;80(3):721–727.
91. Nemoto K, Tateishi T, Ishidate T. Changes in diffusion-weighted images for visualizing prostate cancer during antiandrogen therapy: preliminary results. Urol Int 2010;85(4):421–426.
92. Mueller-Lisse UG, Swanson MG, Vigneron DB, et al. Time-dependent effects of hormone-deprivation therapy on prostate metabolism as detected by combined magnetic resonance imaging and 3D magnetic resonance spectroscopic imaging. Magn Reson Med 2001;46(1):49–57.
93. Dehdashti F, Mortimer JE, Trinkaus K, et al. PET-based estradiol challenge as a predictive biomarker of response to endocrine therapy in women with estrogen-receptor-positive breast cancer. Breast Cancer Res Treat 2009;113(3):509–517.
94. Glunde K, Pathak AP, Bhujwalla ZM. Molecular-functional imaging of cancer: to image and imagine. Trends Mol Med 2007;13(7):287–297.
95. Jordan BF, Runquist M, Raghunand N, et al. Dynamic contrast-enhanced and diffusion MRI show rapid and dramatic changes in tumor microenvironment in response to inhibition of HIF-1alpha using PX-478. Neoplasia 2005;7(5):475–485.
96. Rudin M. Imaging readouts as biomarkers or surrogate parameters for the assessment of therapeutic interventions. Eur Radiol 2007;17(10):2441–2457.
97. Murukesh N, Dive C, Jayson GC. Biomarkers of angiogenesis and their role in the development of VEGF inhibitors. Br J Cancer 2010;102(1):8–18.
98. Hylton N. Dynamic contrast-enhanced magnetic resonance imaging as an imaging biomarker. J Clin Oncol 2006;24(20):3293–3298.
99. Padhani AR, Miles KA. Multiparametric imaging of tumor response to therapy. Radiology 2010;256(2):348–364.
100. Kobayashi H, Longmire MR, Ogawa M, Choyke PL, Kawamoto S. Multiplexed imaging in cancer diagnosis: applications and future advances. Lancet Oncol 2010;11(6):589–595.
101. Padhani AR. Multifunctional MR imaging assessment: a look into the future. In: Koh DM, Thoeny HC, eds. Diffusion-weighted MR imaging. Berlin, Germany: Springer, 2010; 165–180.
102. Miles KA, Williams RE. Warburg revisited: imaging tumour blood flow and metabolism. Cancer Imaging 2008;8:81–86.
103. Dizdarevic S, Peters AM. Imaging of multidrug resistance in cancer. Cancer Imaging 2011;11:1–8.

Novel Oncologic Drugs: What They Do and How They Affect Images

Roberto García Figueiras, MD • Anwar R. Padhani, MBBS, FRCP, FRCR • Vicky J. Goh, MD, MRCP, FRCR • Joan C. Vilanova, MD, PhD • Sandra Baleato González, MD • Carmen Villalba Martín, MD • Antonio Gómez Caamaño, MD • Anaberta Bermúdez Naveira, MD • Peter L. Choyke, MD

RadioGraphics 2011; 31:2059–2091 • **Published online** 10.1148/rg.317115108 • **Content Codes:** BQ MI OI

Page 2060
Typical hallmarks of tumors include *(a)* independence from growth signals, *(b)* insensitivity to growth-inhibitory signals, *(c)* evasion of apoptosis, *(d)* development of a limitless potential for replication, *(e)* development of sustained angiogenesis, and *(f)* tissue invasion and metastasis.

Page 2060 (Table on page 2061)
In current clinical practice, the main classes of NODs include antiangiogenic drugs, antivascular agents, drugs interfering with EGFR-HER2 or KIT receptors, PI3K/Akt/mTOR pathway inhibitors, and hormonal therapies, although the latter constitute a specific class of therapies (4) (Table 1).

Page 2065
In addition, anatomic imaging techniques that use size-based criteria may be insensitive to changes that inform about the overall therapeutic success of cytostatic therapies, since the basic assumption that changes in tumor size reflect biologic activity is violated.

Page 2066 (Figure on page 2066)
Functional imaging techniques, such as perfusion CT, dynamic susceptibility contrast MR imaging, dynamic contrast-enhanced (DCE) MR imaging, or diffusion-weighted MR imaging, provide information on tissue phenotype or behavior. Molecular imaging techniques, such as PET or MR spectroscopy, allow evaluation of cellular and molecular processes by measuring the levels or activities of specific macromolecules or metabolic pathways in vivo (Fig 6).

Page 2086 (Table on page 2086. Figure on page 2087)
By combining data on tumor perfusion and vascularity, cellular density and necrosis, tumor metabolism, and degree of hypoxia together with the receptor expression for the intended target, an "imaging phenotype" of the tumor can be created (Table 9) and one may begin to truly understand which cellular processes are affected by therapy in vivo (Fig 28).